Fall 12-15-2023

Developing Novel Food Packaging Products With High Barrier Properties, Enabled by CNF

Nabanita Das
University of Maine, nabanita.das@maine.edu

DEVELOPING NOVEL FOOD PACKAGING PRODUCTS WITH HIGH BARRIER PROPERTIES, ENABLED BY CNF

By

Nabanita Das

B.S. Shahjalal University of Science and Technology, Bangladesh 2019

A THESIS

Submitted in Partial Fulfillment of the

Requirements for the Degree of

Master of Science

(in Forest Resources: Bioproducts Engineering)

The Graduate School

The University of Maine

December 2023

Advisory Committee:

Mehdi Tajvidi, Associate Professor of Renewable Nanomaterials, Advisor

Islam Hafez, Assistant Professor of Wood Science & Engineering, Advisor

Douglas W. Bousfield, Professor of Chemical and Biomedical Engineering

DEVELOPING NOVEL FOOD PACKAGING PRODUCTS WITH HIGH BARRIER PROPERTIES, ENABLED BY CNF

By Nabanita Das

Thesis Advisor: Dr. Mehdi Tajvidi & Dr. Islam Hafez

An Abstract of the Thesis Presented
in Partial Fulfilment of the Requirements for the
Degree of Master of Science
(in Forest Resources: Bioproducts Engineering)
December 2023

In recent times, plastic has become a highly favored choice for packaging due to its exceptional microbial, damage, and water-resistant properties. However, the alarming rise in plastic usage has led to adverse environmental pollution. This study aims to develop innovative food packaging solutions using renewable and compostable cellulose nanofibrils (CNFs). This thesis comprises two related studies on the barrier performance of novel food packaging materials, including oxygen barrier and oil/grease barrier properties.

The goal of the first study was to enhance the mechanical and barrier properties of the cellulose nanofibril (CNF) films by inducing fibrils orientation for food packaging applications. To attain the alignment, CNF films were produced using an auto dynamic sheet former (ADSF) by varying the wire speeds as well as the solid contents of CNF suspension. The wet films were dried using restrained (Z_Z shrinkage) and non-restrained (XY_Z) methods. The tensile strength and tensile modulus (E) of the ADSF-produced films were tested in the machine and cross-direction and were found to be higher for Z_Z films compared to XY_Z films at 1000 m/min and 1100 m/min

wire speeds with an average anisotropy ratio of 1.4, depending on the drying method. The films made at a wire speed of 1100 m/min exhibited the highest oxygen barrier properties regardless of the drying method. Polarized light microscopy (PLM) was used to quantify the film's orientation but proved inadequate for measuring the alignment of the entire film. The study found that by optimizing the solids content of the CNF suspension and the wire speed of the machine, it is possible to achieve alignment of native CNF films. Applying a shrinkage drying method can further enhance this alignment, leading to the possibility of producing renewable oxygen barrier materials for food packaging applications.

The second study focused on developing a CNF-laminated wood veneer food serving container as an alternative to plastic and PFAS-based paper containers. In this study, two CNF films were attached on both sides of the wood veneer using a food-grade polyamide-epichlorohydrin (PAE) as an adhesive. The containers were formed by hot pressing the wood veneer with CNF films at 140 °C and 160 °C temperature and 1 MPa or 2 MPa pressure for 3 or 5 min. The mechanical properties of the containers were compared with wood veneer hot-pressed at 160°C temperature, 2 MPa pressure for 5 min. The flexural properties of the composites were measured both parallel and perpendicular to the grain direction and showed an impressive increase compared to the wood veneer control sample (without CNF layers). The thermogravimetric analysis (TGA) results showed that the crosslinking between CNF and the PAE was susceptible to degradation at lower temperatures, which may explain- the trend of decreasing peel strength with increasing treatment parameters. The containers showed excellent oil, grease, and water barrier properties, which demonstrate that these CNF-wood veneer composites can be used as safe, eco-friendly food-containers.

DEDICATION

To all those who have ignited and directed the pursuit of my dreams by helping me overcome my limitations, I offer this thesis to your inspiration. I also dedicate this work to the valiant individuals who are tirelessly striving to save humanity.

ACKNOWLEDGEMENTS

I am incredibly appreciative of all the people who supported and assisted me throughout the writing of this thesis in countless ways. To begin with, I want to thank my family from the bottom of my heart, especially my parents, husband, and siblings, whose unflinching support has been priceless. I am indebted to my mother and my husband, Kallol Barai, for their constant love, encouragement, and motivation throughout my challenging period. This accomplishment would not have been possible without their help.

I would like to express my sincere appreciation to my excellent advisors, Dr. Mehdi Tajvidi and Dr. Islam Hafez, whose unwavering dedication and knowledge have been crucial to my scholastic career. I cannot express enough gratitude for the incredible support, wisdom, and guidance that I have received from my mentors. Their unwavering encouragement and insightful knowledge have been significant to my professional and intellectual growth. I am deeply grateful for the care and attention they provided while reviewing my thesis, and their thoughtful feedback significantly improved its quality. Their countless hours mentoring me are a testament to their immense dedication, and I will always be indebted to them for their influence on my academic pursuits. Additionally, I want to express my sincere appreciation to Dr. Douglas W. Bousfield for generously lending his time, suggestions, and guidance amidst his busy schedules.

I am grateful to Dr. Douglas J. Gardner and Dr. Allison Gardner for imparting their knowledge and expertise through their exemplary courses. Their valuable guidance has played a significant role in shaping my research projects, and I will always cherish their contribution to my academic journey.

I am thankful to the PSSP program at UMaine and the USDA McIntire-Stennis program for funding my research.

I extend my heartfelt appreciation to the dedicated individuals and organizations who provided invaluable support for my research. I would like to thank the personnel at the Process Development Center (PDC), SAPPI North America, and Columbia Forest Products Inc. for their essential contributions. Special gratitude goes to Emma Perry, the manager of the School of Biology and Ecology's electron microscopy lab, for generously sharing her expertise and teaching me the intricacies of operating a scanning electron microscope (SEM). Their collective efforts have greatly enriched the quality and depth of my research, and I am sincerely thankful for their assistance.

I feel so thankful for all the amazing people at the Laboratory of Renewable Nanomaterials, including Md. Musfiqur Rahman, Rakibul Hossain, Mamoona Raheem, Dr. Maryam El Hajam, and former lab member Dr. Wenjing Sun. They always supported me and made me feel like part of the team. I also want to give a special shoutout to Maitham Alabbad for being such a good friend and helping me out when I needed it the most.

Finally, I want to express my sincere gratitude to my friends at the University of Maine, who contributed to making my time here memorable and pleasurable. Their companionship has transformed my experience into one that I will cherish forever, making the University of Maine feel like a second home. I would also like to extend my thanks to the Office of International Programs (OIP) for their support in making this possible.

TABLE OF CONTENTS

LIST OF TABLES

LIST OF FIGURES

CHAPTER 1

INTRODUCTION

Modern life cannot be imagined without using plastic food packaging, which can maintain the savor, nutrients, and freshness of food from office lunch sandwiches to meals taken on mountain climbing (Ebnesajjad, 2012), but that also means a considerable amount of plastic waste is generated globally. Unfortunately, only a small percentage of plastic waste is recycled. Around 80% of plastic waste ends up in landfills or nature (Geyer et al., 2017). These plastic wastes find their way into the marine ecosystem in various ways and can come from various sources, including single-use plastic by consumers, coastline transportation, fishing gear, shipping industries, and unmanaged solid waste disposal (Kershaw & Rochman, 2015). Over time, these plastic wastes are converted to micro (< 5 mm) and nano (<1000 nm) plastics (Walker & Fequet, 2023). Depending on the plastic type and sources, the indigestion of microplastics can deteriorate the digestion and reproduction capacity, energy accumulation, and overall well-being of ocean animals and organisms (Horton et al., 2017; Von Moos et al., 2012).To mitigate the detrimental effects of plastic pollution on the environment, it is essential to replace plastic-based food packaging materials with compostable, eco-friendly alternatives that possess excellent barrier properties.

Cellulose Nanofibrils (CNFs) are being studied as raw materials for high-barrier food packaging because of their high mechanical strength, adequate flexibility, high aspect ratio, and ability to form strong entangled fibril networks (Mousavi et al., 2018). CNFs can be extracted from natural sources such as wood and other plant cell walls and prepared by mechanical processes including homogenization, grinding, and refining (Jonoobi et al., 2015). The wider size distribution and tendency to form a denser web-like structure by hydrogen bonds in films make CNFs a potential

candidate for high-barrier food packaging products that can replace petroleum-based packaging materials (Ncube et al., 2020).

This study focuses on the development of CNF films-based food packaging products with high mechanical and barrier properties. The thesis is structured into four chapters as described below:

Chapter 1 (this chapter), sheds light on background and motivation of the research, goal of the thesis, and outlines of the following chapters.

Chapter 2 is aimed at gaining insight into the correlation between the orientation of CNFs within a film and the oxygen barrier properties of the resulting film. In this study, oriented CNF films were produced using an auto dynamic sheet former (ADSF) by varying the solids content of CNF suspension and wire speed in the machine. For drying wet films, two different methods were tested, and the mechanical and barrier properties of the films were evaluated depending on the films' preparation conditions and drying methods. Lastly, the degree of orientation of the ADSF films was determined and the properties of the oriented films were compared with randomly oriented films.

Chapter 3 focused on producing a novel, multi-layer , PFAs-free food serving container from wood veneer by laminating CNF films using a food-grade polyamide-epichlorohydrin (PAE). The containers were prepared in eight different conditions by varying temperature, pressure and press time. The physical, mechanical, thermal and barrier properties of the containers were assessed and compared with commercial paper plates and un-laminated wood veneer containers to ensure their qualities to replace conventional wood based and paper-based food serving containers.

CHAPTER 2

ENHANCEMENT OF CNF FILM'S BARRIER PROPERTIES BY NANOFIBRIL ALIGNMENT

2.1. Introduction

Plastic materials like polyethylene (PE), polystyrene (PS), and polypropylene (PP) are widely used for food packaging across the globe (Ncube et al., 2020). The plastic food packaging industry has seen a surge in demand during the COVID-19 pandemic, especially for single-use containers. These materials are popular because they are affordable, flexible, and highly resistant to chemical, mechanical, and microbial damage. Higher oxygen barrier properties of these plastic food packaging materials help to extend the shelf life of food, preserve its color, odor, and flavor during storage and transportation, reduce the risk of bacterial and fungal attacks, and keep the food fresh (Zabihzadeh Khajavi et al., 2020).

A considerable amount of plastic waste generated globally is not disposed of properly, and a significant portion of it ends up in oceans or landfills (Tucki et al., 2022). There is a risk of harmful chemicals such as carcinogens leaching out from plastic wraps and food containers into the food, posing a threat to human health especially when hot food is served (Geueke et al., 2023).

To meet the demands of contemporary society for efficient packaging materials, while simultaneously being sustainable and renewable, we need to explore new approaches for improving the potential of cellulose-based materials. Cellulose is the most abundant polymer on

earth. β-1,4D-glucopyranose ($C_6H_{12}O_6$) units form cellobiose, and cellulose is composed of the repeating unit of cellobiose (Mariano et al., 2014)

The main two types of cellulose nanomaterials are cellulose nanofibrils (CNFs) and cellulose nanocrystals (CNCs). CNCs have a rod-like structure, mainly produced by acid hydrolysis, and the length and width of CNCs are usually 100 – 500 nm and 3 – 50 nm, respectively (Whba et al., 2022). On the other hand, CNFs have both amorphous and crystalline regions and are produced by high shear forces using a homogenizer or a refiner, among others. CNFs have a length of 500 – 2000 nm and a width of 20 – 50 nm. CNFs have a higher aspect ratio (length-to-width ratio) and are more flexible than CNCs (Xu et al., 2013).

The light weight and high mechanical properties make CNFs a popular choice as a food material (Mörseburg & Chinga-Carrasco, 2009). According to Fujisawa et al., 2016, the mechanical strength properties of a CNF film can be enhanced by its orientation. Various techniques are available to orient CNF films, including moistened film stretching induced by mechanical force (Gindl-Altmutter et al., 2012), stretching of wet CNF film (Sehaqui et al., 2012), and the auto dynamic sheet former (ADSF) approach (Syverud & Stenius, 2009).

The moistened film stretching orientation technique involves cutting strips from the dry film to be stretched by mechanical force. These strips were then attached to pieces of wood on both ends, moistened with water, and stretched using the grips of a universal testing machine. Once stretched, the strips were dried with hot air. While this method was successful in increasing the mechanical properties of the film, it was necessary to regenerate or modify the CNF film surface prior to applying the orientation method. It should be noted that this method cannot induce orientation in the native and untreated CNF film as they are more prone to strain failure before reaching to preferred orientation threshold.(Gindl-Altmutter et al., 2012; Peng et al., 2015).

To achieve an oriented CNF film through wet stretching, the wet film was sliced into strips and secured to the Instron machine's clamps. A force was then applied to partially stretch the strip. Upon completion of the pulling process, the strips were removed in a stretched conformation and dried under stretching conditions (Sehaqui et al., 2012)). While this method can produce mechanically sound CNF films, it is time-consuming and requires further research to achieve industrial-scale oriented CNF films (Gindl & Keckes, 2007).

Films with oriented CNFs were also produced using an auto dynamic sheet former (ADSF), with careful consideration given to the desired grammage and density. The ADSF is a machine that can produce fiber mats by injecting a mixture of fibers and water through a nozzle onto the inside of a rotating, perforated drum. As the drum spins, the fibers align in the direction of rotation (Sunny et al., 2021) and they are dewatered. After producing oriented CNF sheet, the wet sheet was pressed using a blotted paper to remove any excess water before being dried (Petroudy et al., 2017).By adjusting the nozzle, the fiber orientation within a film produced by the ADSF can be enhanced, resulting in notable changes in the film's mechanical properties (Sunny et al., 2021).

The studies referenced above aimed at orienting fibrils in the structure of a CNF film with an ultimate goal of improving mechanical properties. Given the high mechanical anisotropy of cellulose chains (Moon et al., 2011), it is expected that such an orientation may improve the mechanical properties in the direction of the orientation. In general, amorphous regions of polymers do not exhibit significant resistance to the diffusion of small gas molecules, whereas the more tightly packed crystalline regions can indeed impede the path of such molecules(Fukuya et al., 2014). For cellulose nanocrystals, it has been shown that an improved orientation also leads to better oxygen barrier properties (Chowdhury et al., 2018). However, it

remains unclear from existing literature whether a similar effect can be achieved with oriented CNFs.

The tight and layered structure of CNF films resulting from the coalescence of amorphous and crystalline regions in the cellulose assemblies, elongates the diffusion path of oxygen molecules through the thickness of the film leading to a strong barrier for oxygen (Nair et al., 2014). CNF films are known to exhibit superior oxygen barrier properties in the dry state at room temperature (RH < 50% and 25°C). However, the oxygen penetration rate increases as relative humidity increases from 50% to 80% (L. Wang et al., 2020). This is because higher relative humidity can plasticize the CNF based packaging material and increase the free volume through which oxygen can permeate (Bharadwaj, 2002;Dlubek et al., 2002; Muramatsu et al., 2003). The oxygen barrier properties of the CNF films can also vary depending on the drying method. A study done by Hasan et al., 2021, showed that the oxygen permeance through CNF films was lower when the films were dried using a hot press compared to casting and oven drying methods. However, the relationship between the gas barrier properties of the native CNF film and the fiber orientation in the film requires further investigations.

The goal of this research was to develop an understanding of the relationship between the orientation of CNF films and their oxygen permeability. To this end, an automatic dynamic sheet former was used to prepare oriented CNF films at various conditions, which were then tested for their barrier and mechanical properties. In addition, two drying methods were tested, and the degree of orientation was quantified and compared with randomly oriented CNF films.

2.2. Experimental

2.2.1. Materials

The University of Maine's Process Development Center (PDC) provided a 3 wt.% suspension of CNFs at 90% fines, derived from northern bleached softwood kraft pulp through mechanical fibrillation. Fine content refers to the percentage of fibers in a suspension that are smaller than 200 µm in length, with a 90% fine content indicating that on average, 90% of the fibers are smaller than 200 µm (Amini et al., 2020). The fine content was determined by analyzing an image of the CNF suspension with a Compact Fiber analyzer (MorFi, TechPap Inc, Techpap SAS, Gières, France).

More information regarding the production process and CNF characteristics can be found in previously published works (Ghasemi et al., 2017; Johnson et al., 2016; Nazari et al., 2016; Tajvidi et al., 2016).

2.2.2. Methods

2.2.2.1. Preparation of Films

In this study, CNF films of target basis weight of 60 g/m^2 were prepared using two different methods. These methods are vacuum filtration, which was used to prepare control (unoriented) samples, and auto dynamic sheet former (CanPa® Instruments, Quebec, Canada) used to develop oriented CNF films.

2.2.2.1.1. Vacuum Filtration Method

To utilize the vacuum filtration method for film production, the CNF slurry was diluted to 0.3 wt.% by combining with distilled water. Following this, the suspensions underwent a two-minute sonication process using a Branson 450 Sonifier (Branson Ultrasonics Corporation, Danbury, CT, USA). Next, the suspensions were transferred to a planetary mixer (Thinky 310, Thinky

Corporation, Tokyo, Japan) and mixed for one minute at 2000 rpm followed by a defoaming step which was implemented at 2200 rpm for 30 s. Once the suspensions were bubble-free and homogenous, they were vacuum filtered at 381 mm Hg over two Whatman® #5 filter papers of 11 cm diameter and 2.5 µm pore size. The filtration process was halted after 7 min when the time between two consecutive drops was at least 20 s. Finally, the films were cold pressed for 3 min at 0.2 MPa by placing them between two blotting papers to remove the excess water.

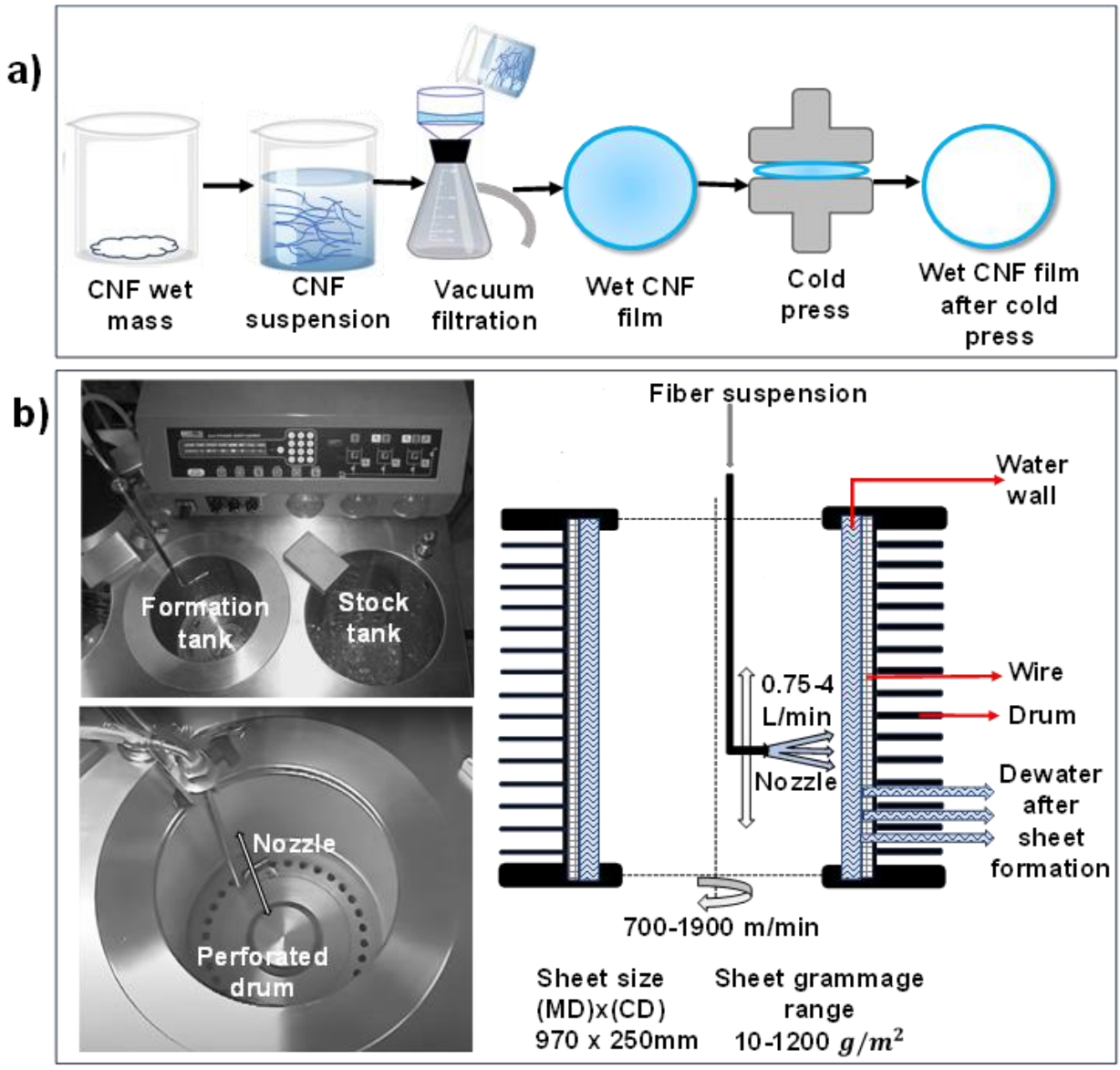

Figure 2.1: Schematic diagram of vacuum filtered CNF film production (a) and a representation of the ADSF drum configuration (b).

2.2.2.1.2. Auto-Dynamic Sheet Former

Using an auto dynamic sheet former (ADSF), oriented CNF films were produced with controlled fiber orientation, like commercial paper making machines. The process involved introducing CNF suspension of varying solid contents (0.1 wt.%, 0.2 wt.%, and 0.3 wt.%) into a stock tank before running the machine.. The instrument comprises a centrifuge drum that is lined with a forming fabric (wire) on the inside. As the centrifuge starts rotating, water is added to it and a wall of water is built up until the wire is entirely submerged in water. Following this, a traversing nozzle sprays the stock against the fabric, to form a layer of fibers. In this study, four different wire speeds (900 m/min, 1000 m/min, 1100 m/min, and 1200 m/min) were used to form the sheets. The stock suspension was deposited onto the wire mesh at a rate of 2.20 L/min using the traversing nozzle with a 3 mm inner diameter to create fibrils layer. After deposition, the dewatering process ran for 4 min at 1400 rpm to produce a wet sheet of CNFs. The sheet could not be produced using 1200 m/min and 0.1 wt.% CNF suspension as the machine could not hold the lighter suspension at the high speed.

After forming the wet sheet, it was delicately positioned onto a Flexiglass surface with two blotting papers carefully resting on top. Filter papers with 11 cm diameter were then precisely placed onto the wet sheet. Another flexible glass sheet was added to the top of the stack before flipping it over and passing it through a two-roller sheet press with a pressure of 0.21 MPa to thoroughly eliminate any excess water. After the cold press, the top glass surface, blotting paper, and wire mesh were removed by flipping the assembly. Finally, the process was concluded by removing the films along with the filter papers from the bottom glass surface by cutting around the filter paper circles. This allowed the transfer of wet sheets onto filter paper. The orientation

direction was marked on the samples, and they were placed in Ziploc bags and stored in a refrigerator for further processing.

2.2.2.2. Film Drying Methods

2.2.2.2.1. Z_Z Shrinkage/Restrained Drying

To dry the film, a pair of filter papers were positioned above and below the wet film. This stack was then placed between two stainless steel plates and heated to 150℃ for a duration of 8 min using a Carver hot-press (Carver, Inc, Wabash, IN) where the platens of the hot-press were only touching the stainless-steel plates without applying pressure. The filter papers were then removed from the film and a pressure of 1.1 MPa was applied for 4 min at the same temperature used for the compaction. This process was found to be effective in minimizing interfibrillar gaps and increasing the density (Hasan et al., 2021) of the film. It is worth noting that when the Z_Z shrinkage method was utilized for drying, the film only experienced shrinkage in the vertical direction and the restraint from the filter paper prevented in-plane shrinkage.

2.2.2.2.2. XY_Z Shrinkage/Non-Restrained Drying

To achieve XY_Z shrinkage drying, the wet film's filter paper was removed, and the film was placed on the surface of a stainless-steel plate. To prevent any pressure impact during the drying process, an aluminum spacer was used between the steel plates. The film was then hot-pressed at 150℃ for 8 min, without any pressure applied. Once dried, the film was pressed again between the steel plates for 4 min at 150℃, using the same pressure as Z_Z shrinkage drying method. The XY_Z shrinkage drying technique resulted in the film's shrinkage in both the vertical and radial directions.

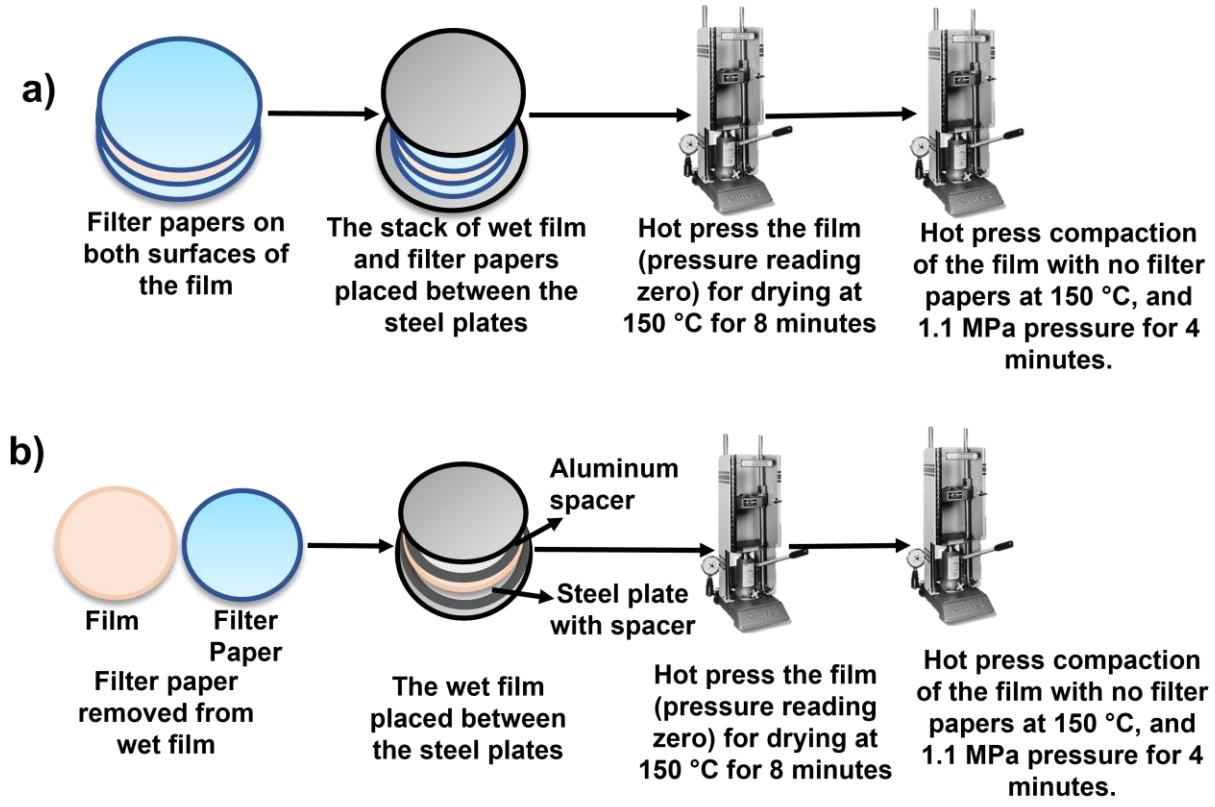

Figure 2.2: Schematic diagram of a) Z_Z shrinkage drying, b) XY_Z shrinkage drying.

2.2.2.3. Characterization

2.2.2.3.1. Mechanical Properties

Prior to testing, the specimens were conditioned in a controlled humidity chamber at 50% relative humidity and a temperature of 23±2℃ for 24 h. To determine how the alignment of CNF films affects their mechanical strength, tensile testing was conducted in the machine and cross directions. In this context, the machine direction is the expected orientation direction parallel to the direction of the ADSF's drum rotation whereas the cross direction is the direction perpendicular to the motion direction. A universal testing machine (Model 5942, INSTRON Instruments, MA, USA) with a 500 N load cell was used to determine tensile modulus (E), tensile strength, and tensile strain. Seven strips measuring 50 mm in length and 10 mm in width were taken from both directions of the films. During testing, the crosshead motion speed was set

to 2 mm/min and the actual gauge length was 20 mm. Tensile strength and modulus results were normalized by the density of the specimens. The density was determined by measuring the dimensions and mass of the samples using a Vernier caliper and an analytical balance, respectively.

2.2.2.3.2. Oxygen Transmission Rate

The oxygen transmission rate (OTR) through the films was determined using a Mocon Ox-tran 2/22 analyzer (Mocon, MN, USA), following the ASTM D3985-05 (ASTM D3985-05, 2010) protocol with a test area of 5.64 cm^2. Prior to testing, samples were conditioned for 6 hours at 80% RH and 23℃ inside the machine. The sensor was cleaned through a "rezero" process with 98% nitrogen and 2% hydrogen gas before the machine recorded the OTR value of the film using pure oxygen gas for 15 min. The test was terminated if the difference between the last measurement and the fifth measurement prior was less than 1%. If the difference exceeded expectations, the machine continued the testing cycle with another "rezero" process after two tests. To account for variation in film thickness, OTR values were normalized, and oxygen permeability (OP) values were determined.

2.2.2.3.3. Birefringence Orientation Index (BOI)

Imaging was conducted using an AmScope polarized light microscope equipped with an AmScope HY-2307digital camera (Model ME50TA, CA, USA). Samples were positioned on a rotating stage with a light source and marked with angles for precise placement. A red filter was utilized as the retardation filter and samples were images between cross polarizers, when oriented in the machine direction and placed parallel to 0° angle. Images were captured at 0°, -45°, and +45° angles by rotating the sample which indicates that the sample was rotated clockwise (+45°) and counterclockwise (-45°) between cross polarizers. Cellulose nanofibrils

exhibit birefringence colors, switching from blue to yellow between -45° and +45° under the polarized light microscope, with the intensity change of the blue color indicating a shift in fiber alignment within CNF films (Ghasemi et al., 2020). The Birefringence Orientation Index (BOI) of the films was calculated using PLM images with ImageJ software (Version 1.44, NIH, Maryland, USA), following a similar method for image analysis and noise removal to produce histogram of the BOI values as indicated in Ghasemi et al., 2020. The BOI values were determined to represent the extent of alignment in a film, estimated from the images of intensity changes in the blue channel between angles using Equation 1.

$$\text{BOI} = \frac{b_{-45^\circ} - b_{+45^\circ}}{b_{-45^\circ} + b_{+45^\circ}} \qquad \text{Equation (1)}$$

where, b_{-45} and b_{+45} are the digital numbers (DN) of blue channel for every pixel (8 bit = 0 – 255) of the RGB images at their respective angles. BOI values range from – 1 to + 1. The +1 indicates the maximum and -1 indicates the minimum alignment in parallel to the machine directions, respectively whereas zero BOI value indicates the random orientation of fibers in the films. To obtain a clearer understanding of the orientation of films, three samples of the same production - conditions films underwent analysis using PLM for BOI calculation. The median BOI values were calculated to minimize the impact of outliers. The resulting noise-free and smooth BOI images were then utilized to generate classified BOI maps using ArcGIS Pro (Version 2.7, ESRI, Redlands, CA, USA).

2.2.2.3.4. Statistical Analysis

The objective of the research was to examine how different wire speeds and solid contents of CNF suspension affect the mechanical and oxygen barrier characteristics of the film. To

accomplish this, a generalized linear model was used to conduct statistical analysis using IBM SPSS Statistics (IBM, Armonk, New York, USA) , with the wire speeds and solid content of CNF suspension being utilized as factors in the analysis. The Tukey Honestly Significant Difference (HSD) test was used to identify any statistically significant differences between the means of different groups, with a 95% confidence interval ($p < 0.05$).

2.3. Results and Discussion

2.3.1. Films Physical Properties

This study utilized the Z_Z and XY_Z shrinkage drying techniques. The Z_Z shrinkage drying involves adhesion between the surfaces of the CNF film and filter paper rather than traditional pressure-based methods, to achieve restrained drying. Whatman® filter papers, which are non-shrinkable when dried but possess an affinity to water, were used to interact with wet CNF films. By cold pressing the wet CNF film with the filter paper, the adhesion between the two layers restricted the in-plane movement of the film without the need for additional pressure. Upon removal of the filter paper, no significant shrinkage in the diameter of the film was observed. In contrast, unrestrained drying involved placing the film directly on a metal plate surface with a spacer, which allowed air to flow through and induce radial shrinkage. Vertical shrinkage was achieved by applying pressure to both restrained and unrestrained films after drying. Refer to Figure 2.3 for a visual representation of the drying methods used in this study and the shrinkage type caused by them.

Upon analysis, it was found that the average linear reduction in diameter after XY shrinkage of the films was approximately 10% compared to the initial diameter of 11 cm. Conversely, the Z_Z shrinkage did not result in any changes in the diameter. The films that experienced Z_Z

shrinkage had an average thickness of 50±10 µm, while the films that underwent XY_Z shrinkage had an average thickness of 60±10 µm.

This result indicates that the drying process for Z_Z shrinkage led to a denser and more compacted film. Ultimately, the average density values of the films for Z_Z and XY_Z shrinkage were determined to be 0.86 g/cm^3 and 0.81 g/cm^3, respectively.

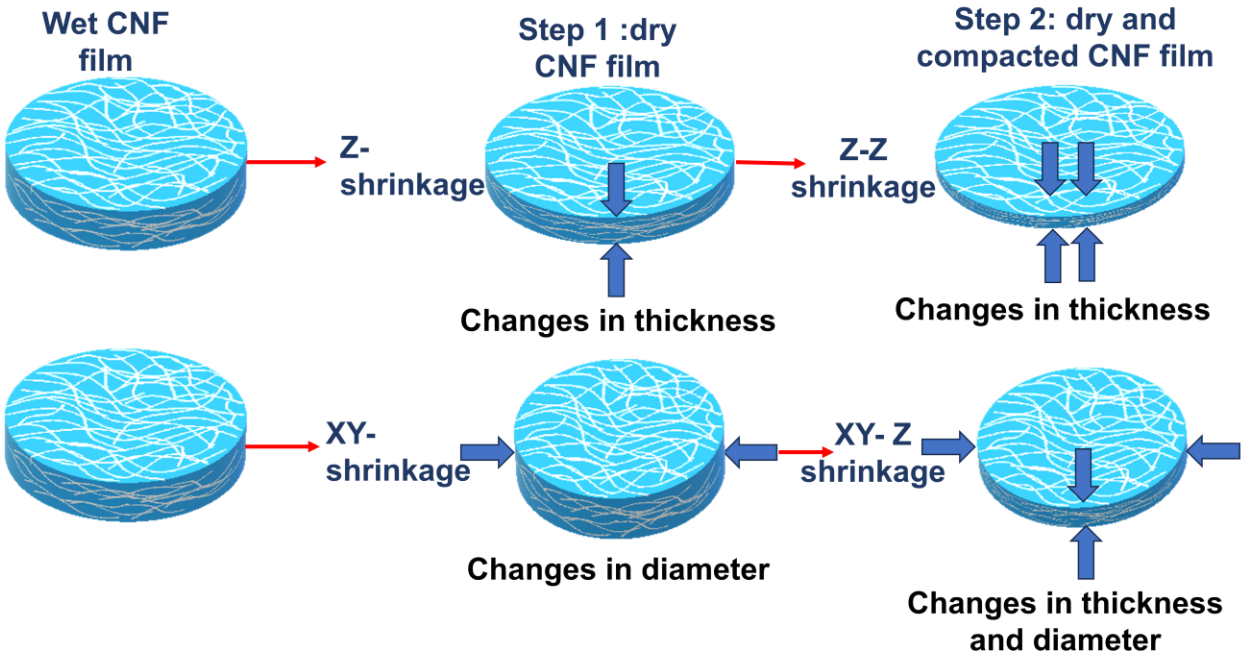

Figure 2.3: The process of producing Z_Z and XY_Z shrinkage drying film.

2.3.2. Tensile Properties

The tensile strength and tensile modulus (E) were normalized by dividing them by the density of the specimens as density data significantly varies among the films depending on the wire speeds and solid content of the CNF suspension. To compare the tensile properties of the ADSF films, they were evaluated against vacuum-filtered films made from a 0.3 wt.% solid content to a basis weight of 60 g/m^2. Due to the random orientation of the fibers in the film, the tensile properties were measured in one direction only.

Table 2.1 and Table 2.2 present the tensile properties of ADSF films that underwent Z_Z shrinkage drying in the machine direction and cross direction. The control vacuum filtered samples displayed a specific strength of 41.8±0.5 (MPa/(g/cm^3)), tensile strain of 5.3±2.6%, and specific modulus of 3151.5±783 (MPa/(g/cm^3)).

Table 2.1: Tensile properties of films made using the Z_Z shrinkage drying method in the parallel direction

Conditions (Wire speed: m/min_ CNF solids: wt.%)	Specific strength (MPa/(g/cm^3))	Tensile strain (%)	Specific tensile modulus (MPa/(g/cm^3))
900_0.1	71.8 (16%)	1.64 (19%)	7117.6 (7.3%)
1000_0.1	82.3 (13%)	1.73 (16%)	7518.2 (7.1%)
1100_0.1	81.9 (24%)	1.82 (31%)	7050.4 (16%)
900_0.2	67.4 (8.0%)	1.55 (13%)	**6742.0 (14%)**
1000_0.2	72.8 (12%)	1.55 (25%)	7613.5 (17%)
1100_0.2	83.6 (8.5%)	1.92 (4.5%)	7135.5 (6.3%)
1200_0.2	76.7 (12%)	1.46(14%)	**8136.5 (11%)**
900_0.3	55.4 (12%)	**1.19 (6.9%)**	6996.9 (24%)
1000_0.3	81.5 (15%)	1.66 (16%)	7870.3 (13%)
1100_0.3	**94.3 (9.0%)**	**1.96 (6.2%)**	7741.8 (13%)
1200_0.3	**54.1 (20%)**	1.26 (20%)	7117.1 (13%)
Control	41.8 (21%)	5.3 (49%)	3151.5 (25%)

*Values in parenthesis are coefficients of variation (CV%)
*The bold numbers represent the highest and lowest values of the specific strength, tensile strain, and specific tensile modulus.

Films prepared at a speed of 1100 m/min and solids content of 0.3 wt.% exhibited the highest specific strength value of 94.3±8.5 (MPa/(g/cm^3)) when tested in the machine direction, while experiencing a 10% reduction in strength in the cross direction. On the other hand, the film prepared at a speed of 1200 m/min and the same solid content had the lowest specific strength value of 54.1±11(MPa/(g/cm^3)) when tested in the machine direction and decreased by 3.1% in

the cross direction. The statistical analysis revealed that the difference between the highest and lowest specific strength values was significant at 95% confidence level.

The highest tensile strain value observed was 1.96±0.12% for the films made at 1100 m/min, 0.3 wt.% in the parallel to the machine direction which reduced to 1.71±0.14% in the cross direction. On the contrary, the lowest tensile strain value found for the conditions 900 m/min and 0.3 wt. % solid content was 1.19±0.08% in the machine direction which decreased to 1.01±0.26% in the cross direction. However, there was no significant difference between the highest and lowest tensile strain values for Z_Z shrinkage drying method.

Table 2.2: Tensile properties of films made using the Z_Z shrinkage drying method in the perpendicular direction

Conditions (Wire speed: m/min_ CNF solids: wt.%)	Specific strength (MPa/(g/cm^3))	Tensile strain (%)	Specific tensile modulus (MPa/(g/cm^3))
900_0.1	81.6 (11%)	2.2 (9.7%)	6530.0 (20%)
1000_0.1	59.3 (35%)	1.59 (44%)	5301.6 (14%)
1100_0.1	76.1 (13%)	1.99 (6.6%)	4803.7 (7.8%)
900_0.2	63.9 (8.5%)	1.78 (5.4%)	**5976.8 (5.2%)**
1000_0.2	66.5 (11%)	1.58 (15%)	5182.8 (9.2%)
1100_0.2	69.6 (7.6%)	1.74 (11%)	5061.9 (5.6%)
1200_0.2	46.9 (13%)	1.02 (30%)	**6664.1 (25%)**
900_0.3	49.7 (13%)	**1.01 (26%)**	7077.9 (16%)
1000_0.3	74.6 (8.3%)	1.63 (11%)	5877.1 (8.4%)
1100_0.3	**84.5 (5.1%)**	**1.71 (8.1%)**	7161.5 (6.2%)
1200_0.3	**52.4 (16%)**	1.13 (18%)	7299.7 (11%)

*Values in parenthesis are coefficients of variation (CV%)
*The bold numbers represent the highest and lowest values of the specific strength, tensile strain, and specific tensile modulus.

In the machine direction, a wire speed of 1200 m/min and solid content of 0.2 wt.% brought about the highest specific E value of 8136.5±883 (MPa/(g/cm^3)), while decreasing by 18% in the cross direction. Alternatively, the ADSF film with a wire speed of 900 m/min and solid content of 0.2 wt.% had the lowest specific E value of 6742±942 (MPa/(g/cm^3)) in the machine direction, which reduced by 11 % in the cross direction. The difference between the highest and lowest specific E values was not statistically significant.

In Table 2.3 and 2.4, the tensile properties of the ADSF films of the XY_Z shrinkage drying method for both the machine and cross directions are presented. The control sample dried using XY_Z shrinkage method showed a specific tensile strength value of 40.3±12 (MPa/(g/cm^3)), a flexural strain of 6.4±2.6%, and a specific E value of 2752.5±647 (MPa/(g/cm^3)).

Table 2.3: Tensile properties of films made using the XY_Z shrinkage drying method in the parallel direction

Conditions (Wire speed: m/min_ CNF solids: wt.%)	Specific strength (MPa/(g/cm^3))	Tensile strain (%)	Specific tensile modulus (MPa/(g/cm^3))
900_0.1	46.2 (23%)	**7.0 (33%)**	3148.8 (36%)
1000_0.1	56.8 (21%)	2.9 (18%)	4077.7 (36%)
1100_0.1	**61.0 (24%)**	3.0 (19%)	5299.4 (31%)
900_0.2	52.0 (14%)	3.5 (25%)	4195.0 (28%)
1000_0.2	53.5 (36%)	3.2 (25%)	5169.4 (25%)
1100_0.2	52.2 (5.0%)	2.7 (19%)	5432.8 (30%)
1200_0.2	52.8 (17%)	3.5 (16%)	**2960.2 (11%)**
900_0.3	**43.4 (18%)**	3.6 (37%)	4377.8 (41%)
1000_0.3	50.2 (16%)	2.5 (4.7%)	3433.8 (44%)
1100_0.3	45.8 (8.1%)	**2.7 (35%)**	**5617.7 (37%)**
1200_0.3	55.0 (2.3%)	3.6 (20%)	4163.5 (29%)
Control	40.3 (29%)	6.4 (40%)	2752.5 (24%)

*Values in parenthesis are coefficients of variation (CV%)

*The bold numbers represent the highest and lowest values of the specific strength, tensile strain, and specific tensile modulus.

For XY_Z shrinkage drying film, films prepared at 1100 m/min wire speed and 0.1 wt.% solids content demonstrated the highest specific strength value of 61±14 (MPa/(g/cm^3)) in the machine direction, but a 22 % reduction in strength was observed in the cross direction. Conversely, the ADSF film with 900 m/min and 0.3 wt.% solid content had the lowest specific strength value of 43.4±8 (MPa/(g/cm^3)) in the parallel direction and an 8% reduction in strength in the perpendicular direction of the machine direction. However, the difference between the highest and lowest specific strength values was not statistically significant.

Table 2.4: Tensile properties of films made using the XY_Z shrinkage drying method in the perpendicular direction

Conditions (Wire speed: m/min_ CNF solids: wt.%)	Specific strength (MPa/(g/cm^3))	Tensile strain (%)	Specific tensile modulus (MPa/(g/cm^3))
900_0.1	50.3 (13%)	**4.3 (35%)**	4111.8 (21%)
1000_0.1	52.7 (8.7%)	3.4 (16%)	5159.3 (28%)
1100_0.1	**47.5 (11%)**	2.7 (21%)	4138.0 (26%)
900_0.2	48.8 (16%)	3.4 (12%)	5406.4 (23%)
1000_0.2	55.1 (7.4%)	2.9 (9.2%)	5077.0 (20%)
1100_0.2	57.2 (12%)	3.0 (16%)	3295.6 (41%)
1200_0.2	52.6 (8.9%)	3.1 (21%)	**4714.8 (24%)**
900_0.3	**39.9 (16%)**	3.7 (46%)	4501.7 (32%)
1000_0.3	49.7 (7.0%)	3.6 (11%)	3400.2 (22%)
1100_0.3	41.5 (6.8%)	**2.7 (17%)**	**4489.0 (16%)**
1200_0.3	42.2 (3.8%)	4.9 (12%)	4009.0 (30%)

*Values in parenthesis are coefficients of variation (CV%)
*The bold numbers represent the highest and lowest values for specific strength, tensile strain, and specific tensile modulus.

Among the films dried using XY_Z shrinkage method, those made at 900 m/min, 0.1 wt.% solid content yielded the highest tensile strain value 7.0±2.3% in the machine direction which was smaller than that in the cross direction (4.3±1.5%). Conversely, the lowest tensile stain value in the machine direction (2.7±0.94%) was found for the films made at 1100 m/min, 0.3 wt.% solid content which did not show much decrease in the cross direction. The highest and lowest tensile strain values for XY_Z shrinkage drying were found statistically different depending on the wire speeds and solid content variation.

The conditions with 1100 m/min wire speed and 0.3 wt.% solid content resulted in the highest specific modulus values (5617.7±2081 (MPa/(g/cm^3))) in the machine direction for XY_Z shrinkage. However, there was a 20% decrease of specific modulus in the cross direction. On the other hand, the film with 1200 m/min wire speed and 0.2 wt.% solid content had the lowest specific modulus value of 2960.2±326 (MPa/(g/cm^3)) in the machine direction. This value increased by 37% in the perpendicular direction of the machine direction. The difference between the highest and lowest specific modulus values was significant. While the reasons for the increased specific modulus in the cross direction have not been fully explored, it is possible that the increased MOE values may be attributed to the layer-by-layer deposition of fibers in the ADSF. This could potentially lead to misalignment of a greater number of fibers in the underlying layers when compared to the rotational direction.

In Figure 2.4 the relationship between rotational speed and solid content and tensile properties is represented for the Z_Z drying method in both testing directions. The films made at the wire speed of 1100 m/min showed statistically higher tensile strength compared to those made at 900 m/min and 1200 m/min whereas they were statistically similar to the 1000 m/min films while testing in both machine and cross directions. For the tensile strain, there was no statistical

difference among the films in the machine direction whereas the cross-direction data showed that the tensile strain could vary significantly depending on the wire speeds and solid content of the films.

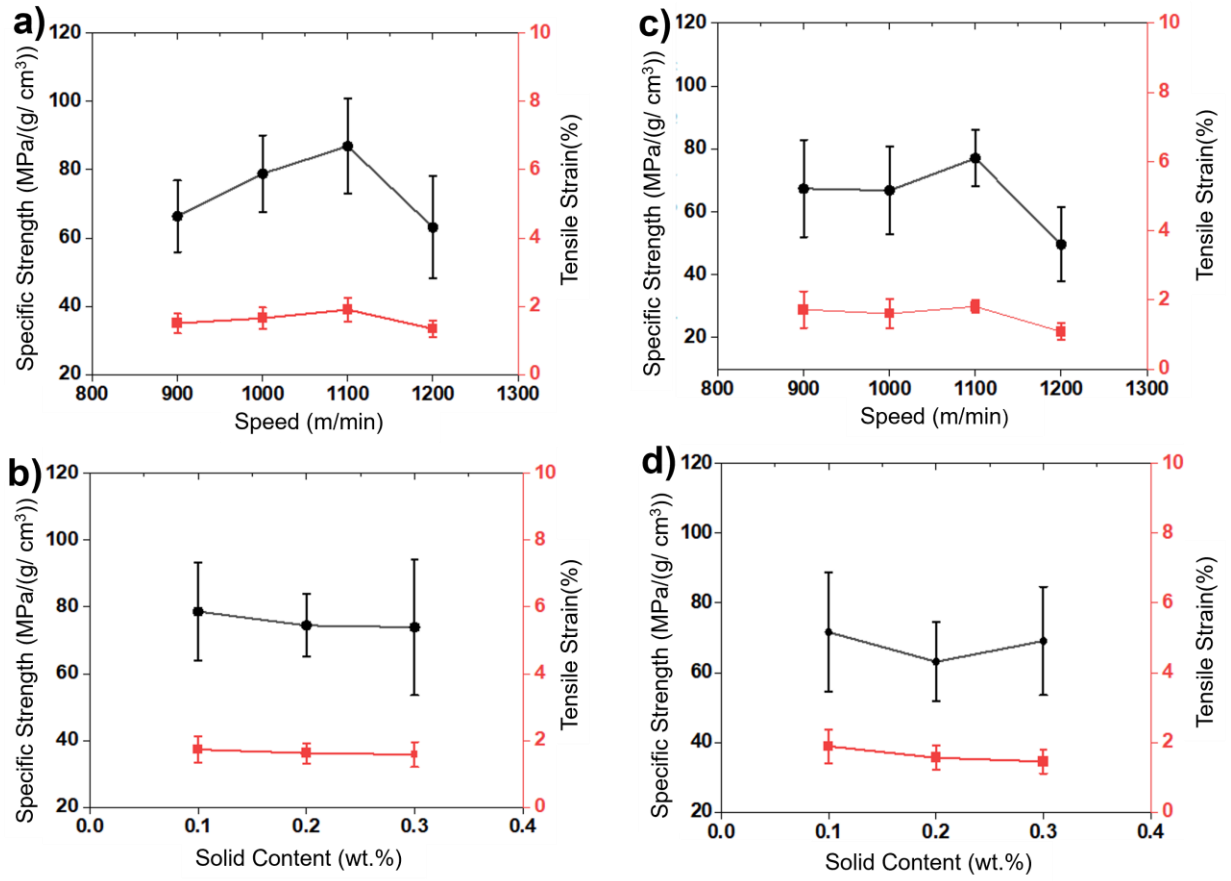

Figure 2.4: Tensile properties as a function of a) wire speed, b) solid content in the parrel direction and tensile properties as a function of c) wire speed, and d) solid content for in the perpendicular direction of samples made using the Z_Z drying method.

Figure 2.5 displays the relationship between rotational speed, solid content, and tensile properties for the XY_Z drying method in both testing directions. The results indicate that the specific tensile strength values were significantly different from each other depending on the wire speed and solid content of the CNF suspension in both directions. The statistical analysis of the tensile

strain revealed significant variations both in the machine and cross directions, which were found to be dependent on the wire speeds and solid content of the films.

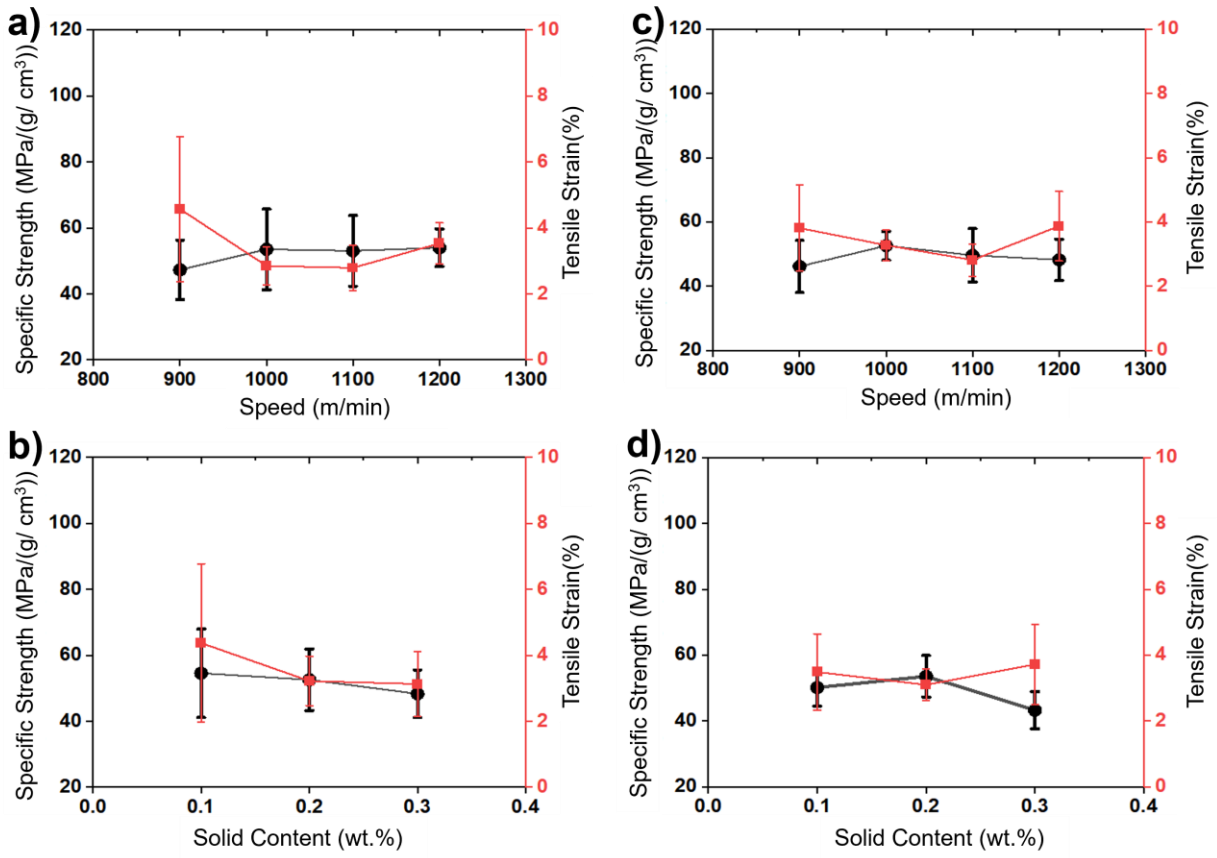

Figure 2.5: Tensile properties as a function of a) wire speed, b)solid content in the parrel direction and c) wire speed, d)solid content for in the perpendicular direction in the XY_Z drying method.

It was determined that both 1000 m/min and 1100 m/min wire speeds are suitable for producing films with favorable mechanical properties, regardless of drying method. Previous research has also indicated that wire speed significantly impacted film's alignment and mechanical properties (Markatos et al., 2018; F. D. Zhang et al., 2014). To enhance alignment and mechanical properties, wire speed optimization is necessary, taking into account the machine's capabilities since optimized wire speeds can both align fibers and hold the bulk of the fiber on the wire mesh (Gigac & Fišerová, 2010). The lowest and highest wire speeds utilized in this study to develop an

oriented sheet were insufficient in holding more fibers on the surface of the wire mash and resulted in a non-uniform fiber distribution on the film surface, which may have contributed to lower mechanical properties.

According to Li et al., 2021, the alignment of fibers in a film can be determined by calculating its anisotropy ratio. This ratio corresponds to the tensile properties of the film in the machine direction versus the cross direction of ADSF, and a value higher than 1 indicates better orientation. To obtain the anisotropy ratio in this study, the specific modulus values of the machine direction were divided by the cross-direction modulus values. Results showed that the film with the maximum anisotropy ratio (1.41) was produced using Z_Z drying at a wire speed of 1000 m/min and the minimum anisotropy ratio (1.06) calculated for 900 m/min, while films dried using XY-Z method at 1100 m/min yielded the maximum anisotropy ratio of 1.38 and those made at 1200 m/min showed the minimum anisotropy ratio of 0.82.

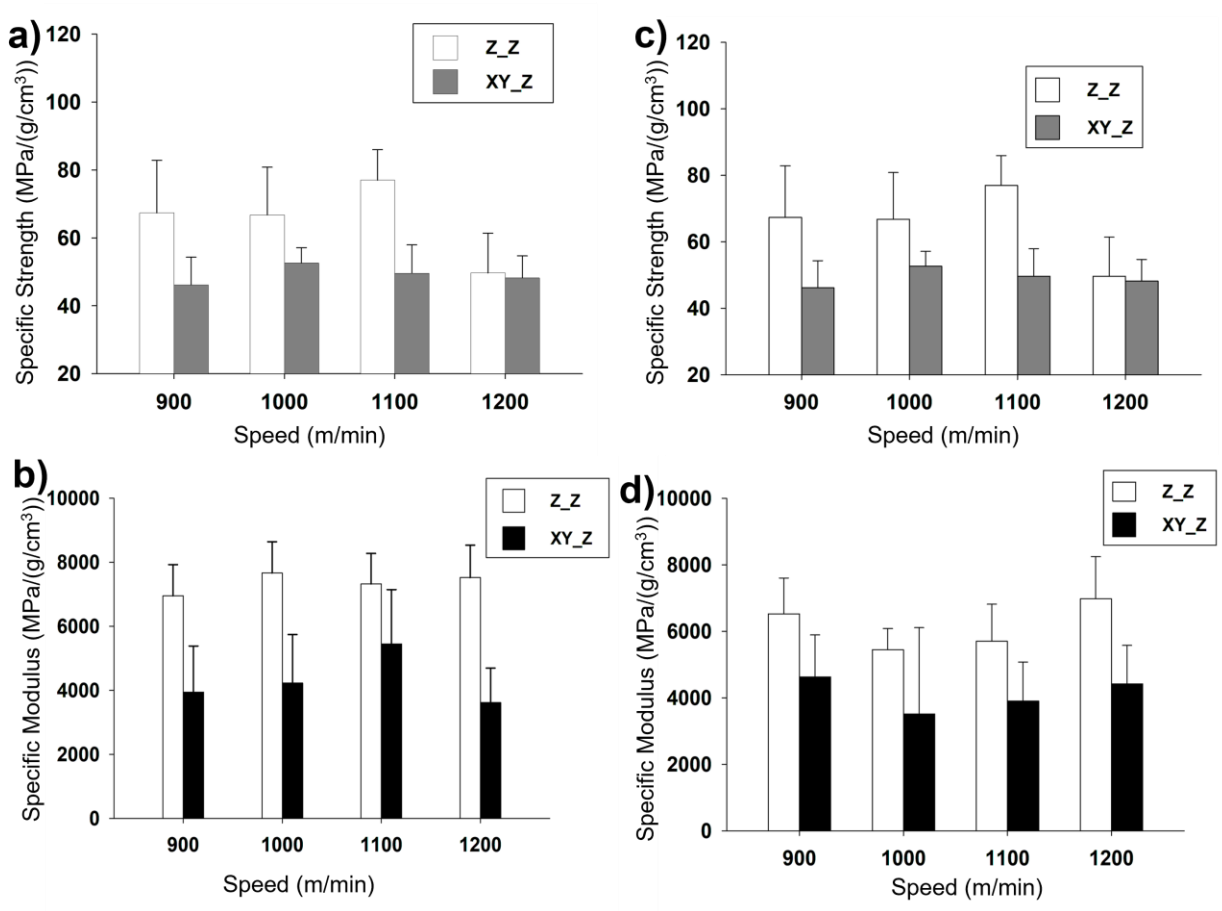

Figure 2.6: Comparison of tensile properties between the drying methods a-b) in the parallel direction, and c-d) in the perpendicular direction depending on the wire speed.

In Figure 2.6, a comparison is presented regarding the tensile properties based on the drying method. It was found that for Z_Z shrinkage drying, the machine direction specific tensile strength of 1000 m/min and 1100 m/min films increased by 47% and 63%, respectively, compared to the XY_Z shrinkage dried films.

The specific strength of the Z_Z shrinkage dried films at 1000 m/min and 1100 m/min wire speed was raised by 46% and 57%, respectively, compared to the XY_Z drying method when evaluated in the cross direction. Additionally, the films showed a similar trend of increased mechanical properties for Z_Z drying in both the parallel and perpendicular direction of machine motion when evaluating the specific modulus values. During unrestrained drying while the film

shrank radially, there is a possibility that the longer and flexible CNF fibers could bend or form coils in the films. When tensile stress is applied, the fibrils within the film may undergo uncoiling or straightening. This increases the tensile strain of the film while reducing stiffness (Ghasemi et al., 2020; Kouko & Retulainen, 2018; Ritchie, 2011). This reason can explain the increase of the tensile strain for XY_Z dried films while reducing the tensile strength compared to Z_Z dried films.

2.3.3. Oxygen Barrier Properties

Food packaging plays a crucial role in maintaining the quality, freshness, and marketability of food products. An essential factor in food packaging is the oxygen barrier property, which prevents oxygen from passing through the packaging material and causing food spoilage and microbial activity.

In Figure 2.7, the oxygen transmission rate (OTR) and oxygen permeability (OP) of ADSF films dried using the Z_Z shrinkage method at 80% RH are displayed. The highest OTR value (17.4±5.1 (cc/m^2.day)) was observed for the conditions of 900 m/min wire speed and 0.1% solid content of CNF suspension while the lowest OTR value (6±0.5 (cc/m^2.day)) was observed for the conditions of 1100 m/min wire speed and 0.1% solid content of CNF suspension. Additionally, the vacuum filtered films exhibited a slightly lower OTR value (5.4±0.1 (cc/m^2.day)) than the ADSF film prepared at 1100 m/min wire speed. One possible reason for obtaining lower OTR values for the control sample is that in the vacuum-filtration process, no agitation or motion was involved which produced very low shear forces during film formation which may have contributed to more uniform and denser films leading to lower OTR value (Osterberg et al., 2013).

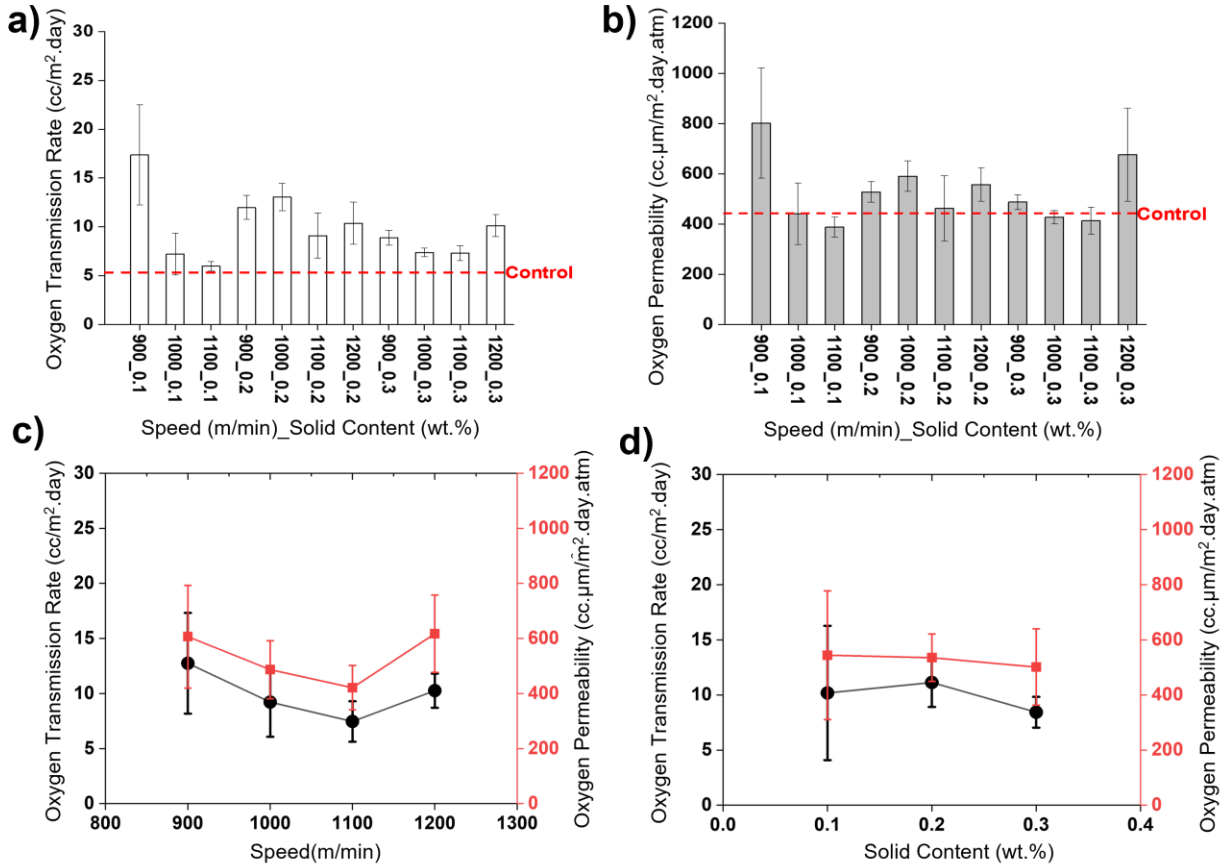

Figure 2.7: a) Oxygen transmission rate, b) Oxygen permeability of the ADSF film and the relationship of oxygen barrier properties with c) wire speed and d) CNF solid content for the Z_Z drying method.

According to Wang et al., 2018, the thickness and relative humidity of a film greatly impact the rate at which oxygen can pass through it. To accurately determine a film's oxygen permeability, OTR values must first be normalized to account for thickness variations. The ADSF films with 0.1% solid content and a wire speed of 1100 m/min demonstrated the lowest OP value of 387.7±40 (cc.µm/m^2.day.atm), while the CNF films with 0.1% solid content and a wire speed of 900 m/min had the highest OP value of 803±220 (cc.µm/m^2.day.atm). It's observable that the OP values of the 1100 m/min wire speed and 0.1% solid content ADSF films showed a 11.4% reduction compared to the vacuum filtered samples.

For Z-Z shrinkage drying, based on wire speed, various differences were observed in ADSF films for oxygen barrier properties. Oxygen barrier properties were lower in the 900 m/min films, whereas the 1100 m/min films presented higher oxygen barrier properties. Moreover, the 1100 m/min films were found to be more oriented than the 900 m/min films, according to anisotropy ratio evaluation. . Through hot press compaction and a more anisotropic fiber alignment, free volume was reduced by increasing packing density, leading to a more tortuous path for oxygen to passage through the film.

The results presented in Figure 2.8 (a-b) illustrate the oxygen barrier properties of the XY_Z shrinkage films. According to the mechanical properties analysis of XY_Z shrinkage films, it was calculated that the 900 m/min films may have a lower anisotropy ratio, suggesting a potential for less orientation in the film. In contrast, the 1100 m/min films demonstrated a higher anisotropy ratio, indicating a possibility of higher films' orientation in the XY_Z shrinkage drying process. To investigate the correlation between CNF alignment in the film and barrier properties, the oxygen barrier properties of the 900 m/min and 1100 m/min films were examined. Furthermore, the 900 m/min, 0.1 wt.% and 1100 m/min, 0.1 wt.% films were selected for oxygen barrier properties testing of the XY_Z shrinkage method due to their higher and lower oxygen permeability values, respectively, for Z_Z shrinkage drying.

It was observed that the OTR of the films made at 900 m/min and 0.1 wt.% was 9.5% higher value than that of 1100 m/min. Additionally, the oxygen permeability values determined by normalizing the OTR values, revealed that the 900 m/min /0.1 wt.% film had a 40.5% higher permeability value than the 1100 m/min / 0.1 wt.% film, which is consistent with the Z_Z shrinkage method findings. The vacuum filtered control sample also demonstrated 4.3% lower oxygen permeability values than the 1100 m/min film, similar to the Z_Z shrinkage drying

method. However, the difference between the oxygen permeability value of control sample and 1100 m/min were not significantly different.

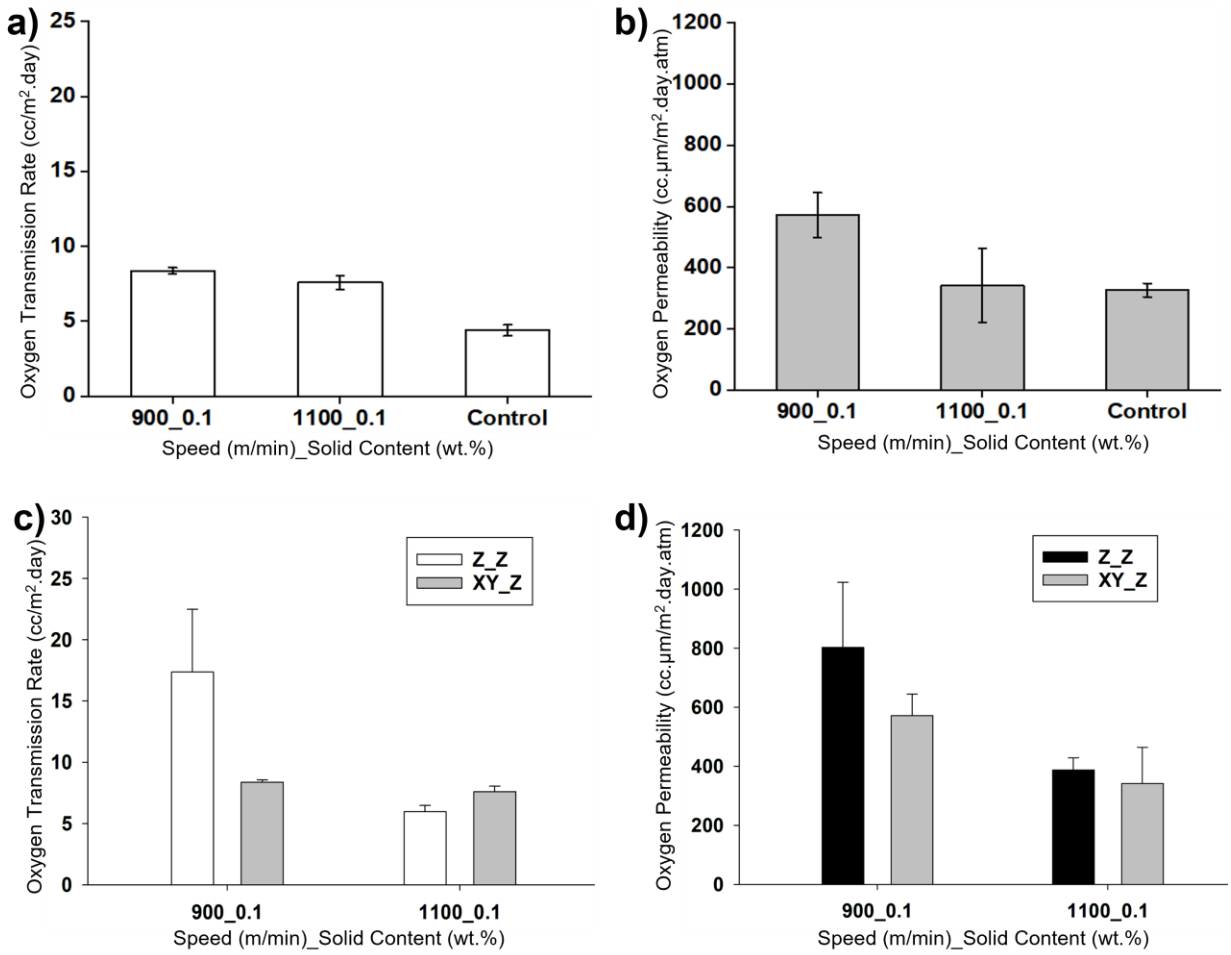

Figure 2.8: a) Oxygen transmission rate, b) Oxygen permeability of the ADSF film for XY_Z drying method and the comparison between Z_Z shrinkage drying method and XY_Z shrinkage drying method depending on c) Oxygen transmission rate, d) Oxygen permeability of the ADSF film.

Figure 2.8 (c-d) indicates the comparison between Z_Z shrinkage drying method and XY_Z shrinkage drying method oxygen barrier properties for 900 m/min, 0.1 wt.% and 1100 m/min, 0.1 wt.% films. For the films made at 900 m/min, 0.1 wt.% it was found that XY_Z shrinkage drying method resulted in the OTR and OP values that were 52% and 29 % lower (improved barrier properties) than the corresponding films dried using the Z_Z shrinkage drying method,

respectively. CNF films can be significantly self-oriented when subjected to un-restrained drying method (Ghasemi et al., 2020) which could contribute to the improvements in the oxygen barrier properties for XY_Z shrinkage drying method.

At a speed of 1100 m/min and a concentration of 0.1 wt.%, the XY_Z shrinkage drying method was found to result in lower OP values by 12%, compared to the XY_Z shrinkage drying method. Though there was so statistical difference found for the OP values of two drying methods while comparing within a specific wire speed. The anisotropy ratio of the film made at 1100 m/min was found to be 1.4 for both drying methods, which suggests that they do not differ in orientation in terms of mechanical properties. Therefore, it is possible that the variance in oxygen barrier characteristics between Z_Z and XY_Z shrinkage film of 1100 m/min wire speed can be attributed to the shrinkage drying process used for each. From the density calculation, it was found that Z_Z experienced a significant increase density, leading to a narrower gas passage pathway in the denser films. As a result, oxygen gas permeance through the films could be reduced.

To gain a better understanding of the correlation between films' orientation and their barrier properties, we further quantified the degree of orientation in the subsequent section. This can provide greater clarity on the connection between films orientation and their barrier properties.

2.3.4. Polarized Light Microscopic Property

Based on the findings of mechanical and barrier properties, it was discovered that the film made with a wire speed of 900 m/min and 0.1 wt.% CNF solid content could potentially have the least CNF orientation, while the film made with a wire speed of 1100 m/min and 0.1 wt.% CNF solid content of could possibly have higher CNF orientation.

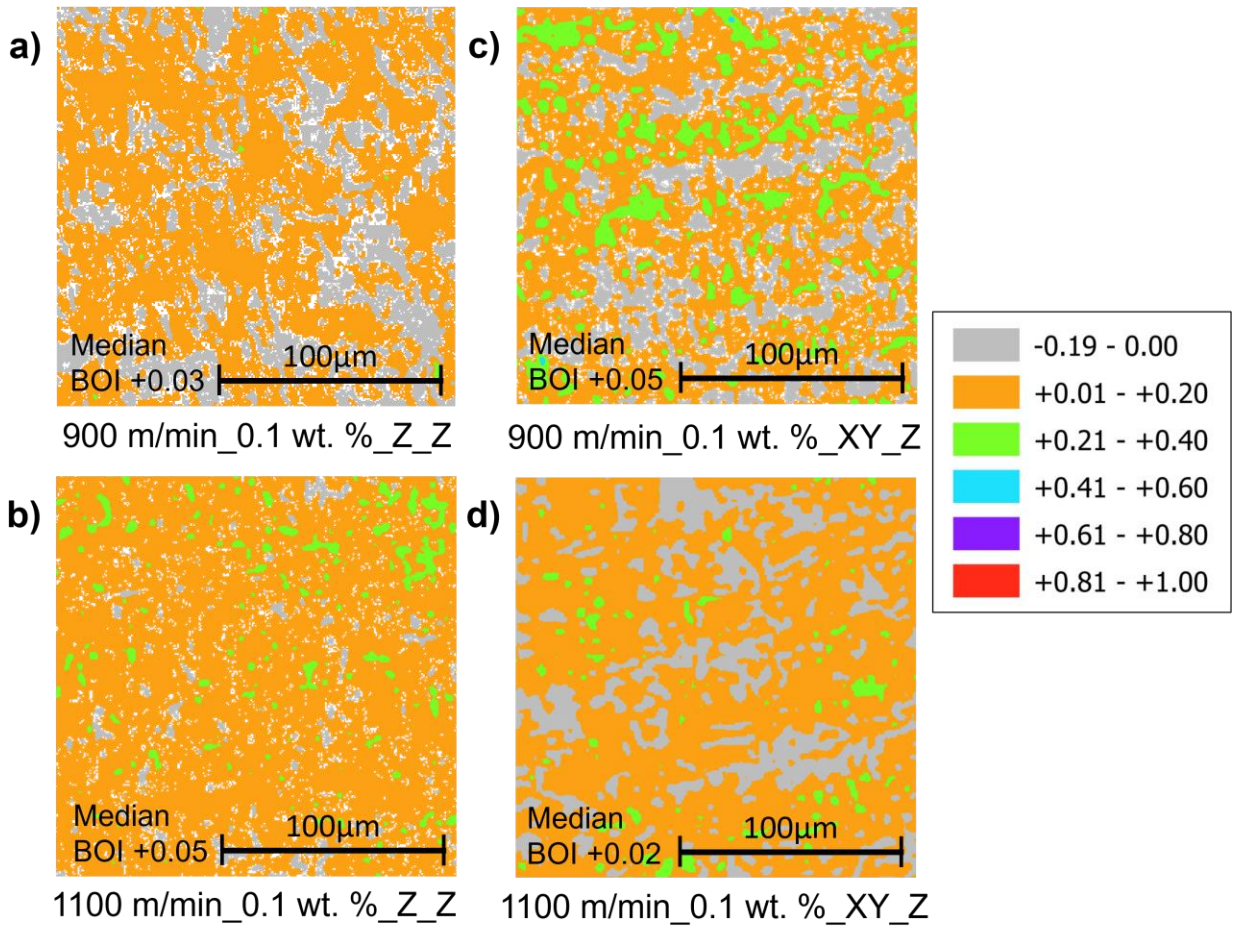

Figure 2.9: The classified map of the BOI index for Z_Z and XY_Z shrinkage drying.

Figure 2.9 reveals the classified maps of BOI values for wire speeds of 900 m/min and 1100 m/min, with a solid content of 0.1 wt. %. These maps indicate the range of BOI values and the level of fiber alignment in the film for both Z_Z and XY_Z shrinkage drying methods. The Z_Z shrinkage drying method revealed a median BOI value of +0.05 for ADSF films with 0.1% solid content and a wire speed of 1100 m/min whereas the median BOI value for the same CNF solids content ADSF film made with a wire speed of 900 m/min was found to be +0.03. The median BOI value for the XY_Z shrinkage drying method was determined to be +0.02 for ADSF films with 0.1% solid content and wire speed of 1100 m/min. However, at a wire speed of 900 m/min

and the same solids content, the median BOI value increased to +0.05 Overall, the changes in median BOI values do not seem to be conclusive, perhaps because of the low level of overall orientation of CNFs in the films.

Comparing the frequency of pixels with higher BOI values in Figure 2.9, however, some general trends can be observed. Firstly, comparing Figure 2.9a with Figure 2.9b indicates that for Z-Z films, the increased wire speed led to better orientation in the direction of wire rotation. This is evident with the relatively lower number of gray pixels (negative values) in Figure 2.9b compared to Figure 2.9a. However, an opposite trend was observed for the XY_Z films where an increase in wire speed led to lower orientation in the machine direction.

The CNFs are able to instigate a significant amount of autogenous orientation in the films when dried un-restrained in all directions (Ghasemi et al., 2020). From the mechanical properties, it appears that the 900 m/min, 0.1 wt.% films had a lower anisotropy ratio, which suggests that there was a low level of orientation. In the Z-Z films that are dried under restraint, it can be expected that the original orientation developed during film formation can be largely retained. However, the unrestrained XY_Z drying may be able to impart additional orientation upon drying. This finding is consistent with a previous study that employed the unrestrained drying method (Ghasemi et al., 2020). It is worth noting that the anisotropy ratio of the 1100 m/min, 0.1 wt.% films indicated better CNF orientation in the films.

Various factors may result in differences between BOI and the anisotropic ratio, including the variation in fiber orientation within the film layers during formation and the limited range of examination with PLM. In the course of ADSF's film production, it was noted that the process involved transverse movement of the nozzle to spray the fiber suspension and form a fiber mat of

the required thickness, which entailed layer-by-layer fiber deposition. This technique could potentially result in fiber misalignment within the film analyzed by PLM.

2.4. Conclusions

In this study, cellulose nanofibril (CNF) films were prepared in a two-step process involving a formation process followed by a drying technique different: We used an auto dynamic sheet former (ADSF) to form the wet mats and either an induced shrinkage drying technique or a restrained (no in-plane shrinkage) technique. The XY_Z films exhibited a 10% reduction in diameter compared to their initial wet sizes, while the Z_Z film showed no significant change in diameter. Additionally, the density of the Z_Z shrinkage films was increased 6.2% in comparison to the XY_Z shrinkage films. The optimized wire speeds and solid content in the ADSF process resulted in higher mechanical strength and tensile properties for the restrained Z_Z drying, whereas the non-restrained XY_Z drying method was able to increase the tensile strain properties of the films. The anisotropy ratio indicated that it is possible to achieve relatively oriented native CNF films by optimizing the wire speed and solid content of the suspension.

The anisotropy ratio calculated for the film produced at the optimized wire speed showed a correspondingly lower oxygen permeability value. This finding suggests that the relatively high degree of orientation in the CNFs could potentially enhance the barrier properties of the film. Considering both drying techniques, 1100 m/min films were able to resist more oxygen than 900 m/min films. To gain a more comprehensive understanding of the degree of orientation within the film, polarized light microscopy (PLM) was employed for imaging. However, PLM images were highly localized, providing insights into only a small area, making it challenging to assess the orientation of fibers across the entire film and relating those to the barrier properties

Nevertheless, the anisotropy ratio obtained from mechanical testing and differences in oxygen barrier properties offer substantial indicators of the film's internal orientation.

Overall, this research reveals the optimized relationship between the wire speed in ADSF and the solid content of native CNF, leading to the production of relatively oriented CNF sheets. It also explains how the shrinkage drying method and fiber orientation collectively impact the mechanical and barrier properties of CNF films, making them a promising choice for food packaging materials, contributing to our efforts to combat plastic pollution and protect the environment.

CHAPTER 3

MULTI-LAYER OIL AND WATER-RESISTANT FOOD SERVING CONTAINERS MADE USING CNF-LAMINATED WOOD VENEER

3.1. Introduction

In recent times, the use of plastic food containers for delivery and takeout meals has seen a significant surge, particularly with the advent of online meal ordering and delivery services. Plastic serving containers and cutlery offer expedient and cost-effective meal-serving options that are quick and easy to use (Razza et al., 2009). However, these conveniences come at the price of increasing greenhouse gas emissions and plastic waste generation (Gallego-Schmid et al., 2019). In addition, plastic food containers have the potential to cause negative effects on human health such as congenital anomalies, immunodeficiency, etc. because of the tendency to release toxic compounds like phthalates into food (Rustagi et al., 2011). The rising concerns with the use of plastic food serving containers have made it high time to shift everyone's interest toward "greener" and more sustainable alternatives to traditional food packaging materials.

As people seek more environmentally friendly alternatives to plastic food packaging, molded fiber and paper-based food containers have gained popularity. Molded pulp products are green products that are produced from mixing the recycled or neat natural fibers with water and forming the mixture into desired shape with a subsequent drying method (Debnath et al., 2022; Didone et al., 2017; Su et al., 2018). Although they offer the benefits of being biodegradable and potentially recyclable, they do have several limitations including challenges with resistance to oil and grease, recycling, and high energy consumption during manufacturing, restricting their use

as food serving containers. Commercially, these products were treated with fluorocarbons such as per- or poly-fluoroalkyl substances (PFAs) to impart oil and grease resistance in the paper-based food containers (Tayeb et al., 2020). However, these fluorocarbons are linked to life-threatening diseases in humans such as cancers and liver problems (Tyagi et al., 2019). Research has been conducted to find alternatives to PFAs coating using non-toxic, biodegradable materials such as starch and montmorillonite (Olsson et al., 2014), chitin (Kjellgren et al., 2006), sodium alginate (Jost et al., 2014), etc. Though the global market of ecofriendly, grease resistant paper products is increasing and is predicted to reach $1 billion by 2025 (Acumen,2019), they are not still competitive with plastic-based containers which are anticipated to have a market size of around $113 billion by 2025 (Grand view research,2019).

Cellulose is one of the most plenteous organic polymers that can serve as a raw material for environmentally safe and biodegradable food serving containers. The development of purification processes, along with energy and cost-saving pulping technology, has made wood the primary source of cellulose (Isogai, 2018). Cellulose characteristics and reaction mechanism are directed by several factors such as interactions among the molecules, the arrangement of functional groups on the repeating units as well as across the chain structure of polymer but in general, the abundance of hydroxyl groups governs cellulose reactivity and physio-mechanical properties (Klemm et al., 2005).

Cellulose nanofibrils (CNFs) are generally produced by the mechanical disintegration of delignified and bleached plant cell walls. The remarkable characteristics of, including their high surface area (depending on the CNFs preparation method), lightweight nature, and impressive mechanical properties, make them a highly desirable form of cellulose for many applications. With more accessible hydroxyl groups on their surface, CNFs exhibit exceptional adhesion, self-

assembly and barrier properties. Due to these distinctive features, CNFs are rapidly gaining recognition as a versatile and promising raw material for a wide range of applications from being used as binder in composites system to materials for barrier coating applications (Amini et al., 2020; Tayeb et al., 2018). Compared to cellulose nanocrystals (CNCs) that are mainly produced through acid hydrolysis of cellulosic fibers, CNFs have a higher aspect ratio (Yook et al., 2020), which also helps CNF films in resisting air and grease as the grammage (basis weight) increases (Amini et al., 2020). The hydrogen bonding between the CNFs' hydroxyl groups is another major reason for their excellent barrier properties (Tayeb et al., 2018). For these causes, food containers made of CNFs are promising and motivate further investigations. A study by Hossain et al., 2021 found that wood flour and CNF composites coated by a layer of CNFs or lignin-containing CNFs (LCNFs) have excellent grease barrier and mechanical properties, making them a viable option for PFAs-free, oil-resistant commercial food serving containers compared to molded pulp products.

An alternative to using deconstructed wood flour bonded with CNFs as the substrate for a food-serving container, it can be hypothesized that a thin layer of wood veneer, a commercially available wood product can also be used for food serving applications especially for shallow tray-like containers where low flexibility of wood is not an issue. However, wood veneer's orthotropic nature, renders it weaker in the perpendicular to grain direction and causes excessive bending a premature fracture (Ross, 2021). Moreover, the other drawbacks of wood veneer are its porosity to allow the passage of oil and grease, water absorbance, vulnerability to bacterial growth and possibilities of extractives leaching to food, making it unsuitable for use as food serving containers (Debeaufort, 2021). This study focused on a composite laminate system comprising of CNFs (derived from bleached Kraft pulp) and yellow birch wood veneer.

Polycup^{TM}, a food-grade polyamide-epichlorohydrin (PAE) was used to bind the layers of CNFs to the veneer. A comprehensive study was designed to assess the composite's physical, mechanical, morphological, thermal, and barrier properties, as an alternative food serving container. Finally, a thorough analysis was performed to compare the performance of this food-serving container with existing commercial food serving containers.

3.2. Experimental

3.2.1. Materials

The University of Maine's Process Development Center (PDC) produces CNFs without significant surface charge resulting from the absence of chemical treatment during production (Tajvidi et al., 2016). CNFs from the University of Maine's PDC were used in this study. The CNF suspension used in this work had 3 wt. % solids content and 90% fine content (around 90% fibers are shorter than 200 microns). The characteristics of the CNF utilized for this research have been previously published (Ghasemi et al., 2017; Johnson et al., 2016; Nazari et al., 2016). Yellow birch (*Betula alleghaniensis*) wood veneers provided by Columbia Forest Products LLC, Presque Isle, ME, USA, were used in this study. Food -grade PAE (Polycup^{TM} 9250) of 36 wt.% solids content used as a crosslinker was generously supplied by Solenis LLC, Wilmington, Delaware, USA.

3.2.2. Methods

3.2.2.1. Fabrication of the food serving containers

In this experiment, yellow birch wood veneer was cut into an 11 cm diameter (94.98 cm^2 area) circles. The thickness and weight grammage of the wood veneers were 0.61 (±0.04) mm and 448.5 g/m^2, respectively. The cut veneer was then treated in a water bath at around 25°C for 24 h to make the veneer more flexible to form into the desired shape at the end.

In another setup, two CNF films of 80 g/m^2 were produced using a vacuum filtration process. To this end, a 0.5 wt.% CNF suspension was sonicated for 2 min at 90% amplitude using a Branson 450 Sonifier (Branson Ultrasonics Corporation, Danbury, CT) and then placed in a planetary mixer (Thinky 310, Thinky Corporation, Tokyo, Japan) for one minute and to defoam for 30 s at 2000 and 2200 rpm, respectively. After that, the suspension was vacuum filtered at 381 mm Hg over a polyester mesh filter screen with an average pore size of 41 µm and an overall diameter of 11 cm for 7 min to form a wet CNF film with the target dry thickness of 80 (±2) µm.

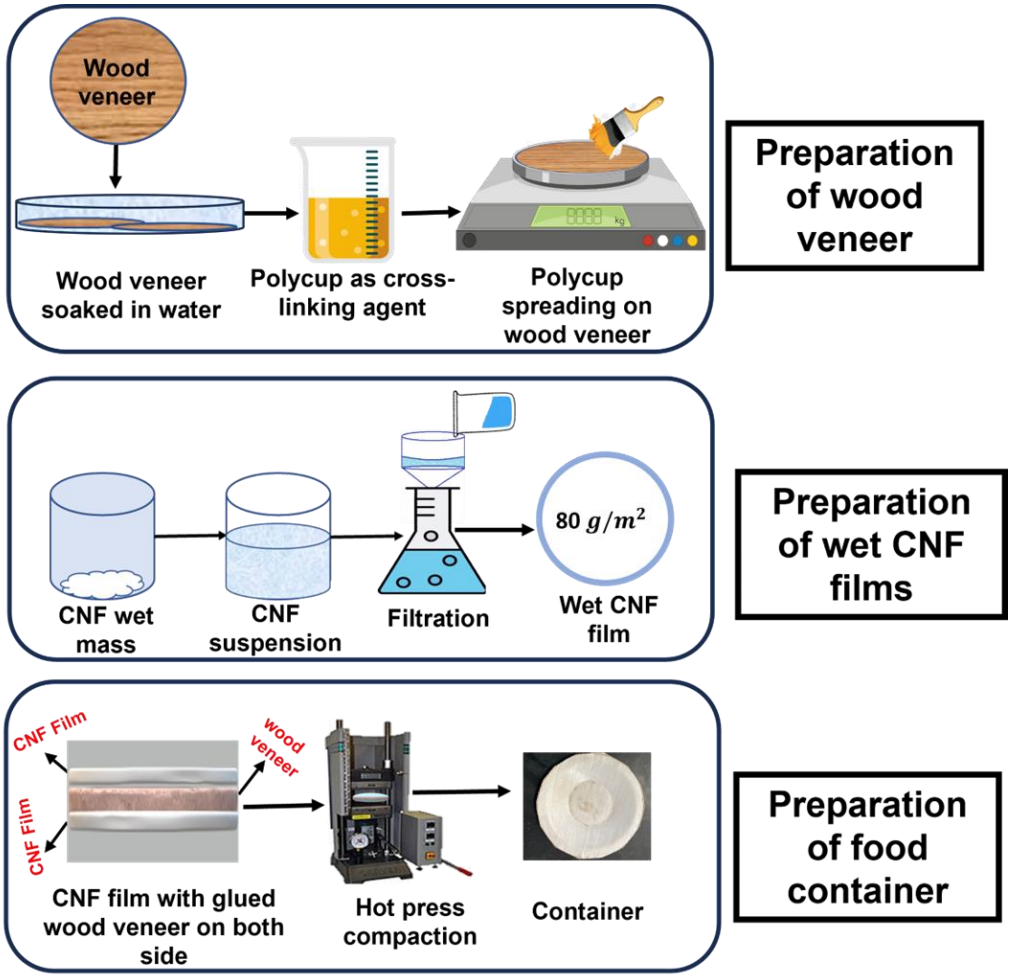

Figure 3.1: Schematic diagram of the fabrication process of oil and grease resistant food serving container via vacuum filtration method and hot press compaction.

The Polycup of 36 wt.% solid content was spread on each side of the wood veneer (12.28 g/m^2 on each side). Using the Polycup density and dimensions of the bond area, the average thickness of the glue line was calculated using the following equation and was found to be 14 µm.

$$\text{The Thickness of The Glue Line} = \frac{Volume\ of\ the\ Polycup\ (cm^3)}{Area\ of\ the\ veneer(cm^2)} \quad \text{Equation (1)}$$

Hereafter, the CNF films were placed on both sides of the wood veneer and hot pressed at 140℃ or 160 ℃ temperature and 1 MPa or 2 MPa pressure for 3 min or 5 min to form the container in the form of a flat sheet. Figure 3.1 presents the schematic diagram of the setup and Table 3.1 lists the formulations produced.

Table 3.1: Formulation codes of oil and grease resistant food serving containers.

Formulation	Time (min)	Temperature (℃)	Pressure (MPa)
1-1-1	3	140	1
1-1-2	3	140	2
1-2-1	3	160	1
1-2-2	3	160	2
2-1-1	5	140	1
2-1-2	5	140	2
2-2-1	5	160	1
2-2-2	5	160	2

3.2.2.2. Characterization

All samples were conditioned at 50±2 % relative humidity for 24 h at 23±2°C before testing in a conditioning chamber, except thermal stability analysis samples. The solids content and density

of the samples were measured by determining the mass and dimensions of the samples using an analytical scale and Vernier caliper. After dividing the conditioned mass by the calculated volume, the densities of the samples were determined, and the average density of the samples was found 0.96 g/cm^3. In addition, the containers were characterized by examining the adhesive strength between the layers, analyzing the qualitative nature of the failure, evaluating the thermal degradation of the components, and assessing oil and water barrier properties. Figure 3.2 summarized the characterization method employed in this study.

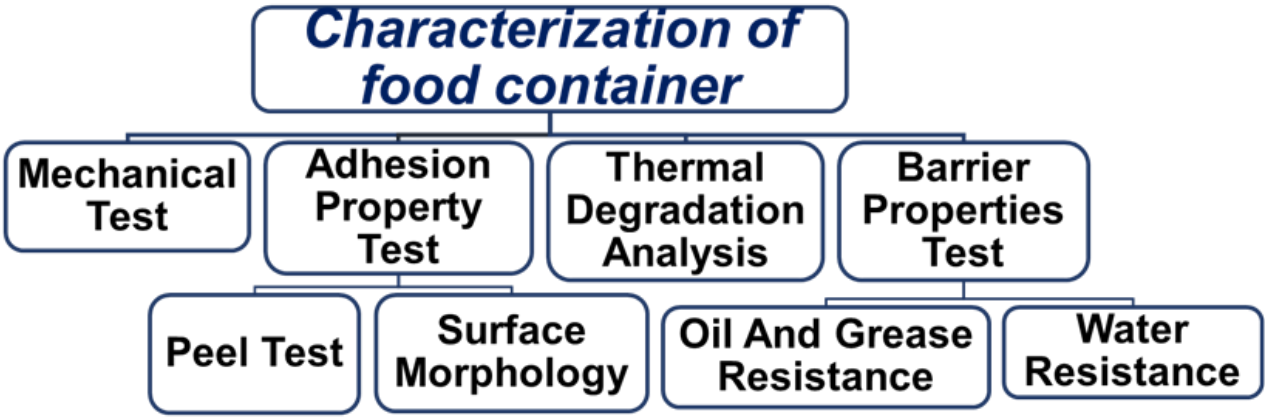

Figure 3.2: Diagram listing the characterization methods of the composite.

3.2.2.2.1. Mechanical Properties

The bending strength of the food serving container was determined by performing a three-point bending test. An Instron mechanical testing machine with a 500 N load cell (Model 5942, Instron Instruments, Norwood, MA) was used to perform the flexural testing following the ASTM standard D790 (ASTM, 1997) with modifications. Seven specimens, each measuring 8 cm in length and 1 cm in width, were cut using an FSL Muse Core Desktop CO2 Laser Cutter (Sandhill Road, Las Vegas, NV) from each formulation of the circular composite materials in both the parallel and perpendicular directions to the wood veneer fibers. The results were then compared with wood veneer specimens of the same dimensions, hot-pressed at a temperature of 160°C and

a pressure of 2 MPa for 5 min as control. The span length was 60 mm, and the crosshead speed of the machine was 5 mm/min during the test. The specific flexural strength, flexural strain, and specific modulus of elasticity (MOE) were determined to understand the stress-strain behavior of the composite.

A peel test was conducted to assess the adhesive strength of the CNF film and wood veneer bond following the ASTM standard (ASTM, D1876). Circular samples of each formulation were produced by applying glue to half of the wood veneer surface, which was then pressed using a hot press. At least five strips, measuring 5 cm in length and 1.5 cm in width, were cut from the circular samples, ensuring both glued and non-glued sides were included. The peel test was performed using the same Instron testing machine described above. The specimens were clamped in the machine's grip by their unbonded ends and pulled at a crosshead speed of 2 mm/min. From the test results, the specific maximum peel strength of the adhesive was determined. The equation of calculating specific maximum peel strength is given below:

$$\text{Peel Strength} = \frac{Maximum\ peeling\ load\ value(N)}{Width\ of\ the\ specimen\ (mm)} \qquad \text{Equation (2)}$$

3.2.2.2.2. Thermogravimetric Analysis (TGA)

Thermogravimetric analysis (TGA) was carried out to evaluate the thermal stability of Polycup, CNFs, and CNFs with Polycup, to understand the thermal degradation behavior between the nanocomposite layers using a TGA Q500 (TA Instruments, New Castle, DE). For each component, three specimens were used, each weighing between 5 and 15 mg. The TGA was conducted under an air atmosphere with a flow rate of 40 mL/min, and the temperature gradually increased to 600 °C at a rate of 10 °C/min. From the resulting TGA and derivative weight loss (DTG) curves, the average peak temperature and onset temperature were calculated.

3.2.2.2.3. Scanning Electron Microscopy (SEM)

To examine the adhesion quality between the layers of the composite, the surface morphology of the bond line between wood veneer and CNF film was assessed after failure. The bonded surfaces of these materials were compared to non-glued veneer surfaces after a peel test using a Zeiss Nvision 40 scanning electron microscope (Oberkochen, Germany). Both the wood veneers and CNF films were attached to aluminum stubs using conductive tape and then coated with a thin layer of gold-palladium to increase the conductivity of the samples' surface. The coated samples were imaged under SEM at an accelerating voltage of 3 kV.

3.2.2.2.4. Oil And Grease Resistance

TAPPI T 559 cm-12 (TAPPI, 2012) standard, generally known as "kit test" was followed to determine the oil and grease resistance of the composite food serving containers and the results were compared with the commercial paper plate. The test procedure was accomplished using a series of numbered reagents (1-12) depending on the surface tension and aggressiveness of the reagents. The highest number (12) represents the most aggressive reagent that remained on the surface of the sample, while the lowest number (1) represents the least aggressive reagent. The reagents for the kit test were prepared by mixing castor oil with toluene and n-heptane.

Five conditioned specimens were tested from each formulation for oil and grease resistance using kit number 1 to 12. The reagents were dropped onto the specimen from a height of around 13 mm using an eyedropper and removed quickly after 15 s using a cotton ball. The tested area was examined immediately to detect any darkening on the test area. The test was considered "passed" if the highest kit number was unable to penetrate the surface of the specimen and leave a dark mark.

3.2.2.2.5. Water Resistance

The water absorptiveness of the food serving containers was measured by following the modified TAPPI 441 om-09 (TAPPI, 2009) standard. The test specimens were conditioned prior to Cobb test and sized into a 77.8 cm^2 area. The preconditioned samples were then weighed on an analytical balance and the metal ring of the Cobb tester was placed on the specimen. A soft nonabsorbent gasket with the same internal diameter as the ring was placed between the metal ring and the specimen to prevent water leakage. The cobb ring was then fastened firmly, and 77.8 ml of water was poured into the ring for 1200 s.

At 10±2 s before the expiration of the predetermined test time, the water was removed from the ring, and the wet face of the specimen was placed on a blotting paper. Another sheet of blotting paper was placed on the top of the specimen, and excess water was removed by rolling a smooth-faced stainless-steel roller with a width of 20 cm and a weight of 10±0.5 kg.

The wet specimen was then reweighed to measure the weight difference between the conditioned dry specimen and the wet specimen to the nearest 0.01 g. Equation 3 was used to determine the water absorbance value (Cobb value) in grams per square meter:

$$\text{Water Absorbance Value} = \frac{Wet\ sample\ weight\ (g) - Conditioned\ dry\ sample\ weight\ (g)}{Test\ surface\ area (m^2)} \quad \text{Equation (3)}$$

3.2.2.2.6. Statistical Analysis

Statistical analysis was conducted using RStudio software (RStudio, PBC in Vienna, Austria). The flexural and peel test data were analyzed through a full factorial analysis, while a one-way analysis of variance (ANOVA) was used for the Cobb test data. Subsequently, Tukey's Honestly Significant Difference (HSD) test was employed to determine any statistically significant differences between the means of different groups. All statistical analyses were done at 95% confidence level ($p < 0.05$).

3.3. Results and Discussion

3.3.1. Flexural Properties

Adequate mechanical strength and stiffness can ensure a food serving container's durability, stackability and safety from hot food spillage. The thickness and basis weight of the food serving containers were 0.63(±0.01) mm and 690 g/m^2, respectively. The density of the samples was analyzed in both the parallel and perpendicular direction to the wood fiber alignment. To determine statistical differences in the two directions among the mechanical test data of the formulations, analysis of variance (ANOVA) was conducted. Findings revealed that pressure caused variations in density data in both parallel and perpendicular directions among the formulations. Furthermore, density differences were observed among the formulation tested in the perpendicular direction also because of the interaction between time and temperature.

The flexural strength and modulus of elasticity (MOE) data were normalized by dividing them by the density of the specimens. Flexural strength determines the amount of applied stress a specimen enables to carry before breaking, and stiffness indicates the deformation resistance of a specimen when a load is applied for bending.

The mechanical properties of the composites were compared with a wood veneer hot pressed at 160°C and 2 MPa for 5 minutes. The density, specific flexural strength, flexural strain, and specific MOE values of the control sample were statistically different from the composite samples prepared under the same conditions and using the same parameters at significance level of 0.05. This difference can be attributed to the addition of CNF layers (80 g/m^2) on both sides of the veneer. Figure 3.3 represents the bending properties of the composite in the parallel to grain direction and compares them with the control sample. Figure 3.4 illustrates the comparison of

flexural properties of the formulations with the those of the control samples in the perpendicular to grain direction.

From the bending test, the formulation 1-1-1 (144.3± 9.2 (MPa/(g/cm^3)) and the formulation 2-1-2 (128.0 ± 6.4 (MPa/(g/cm^3)) had the highest and lowest specific flexural strength, respectively in the parallel direction (Figure 3.3(a)). The factorial design of the formulations showed that pressure and the interaction of time and temperature had a significant impact on the specific strength values in the parallel direction. On the other hand, the specific flexural strength in the perpendicular direction was found to be the highest for the formulation 1-2-1 (80.3 ± 4.8 (MPa/(g/cm^3)) and the lowest value was for the formulation 2-1-1(69.0± 3.3 (MPa/(g/cm^3)) (Figure 3.4 (a)). No statistical difference was found among the formulations for the specific strength values in the perpendicular direction.

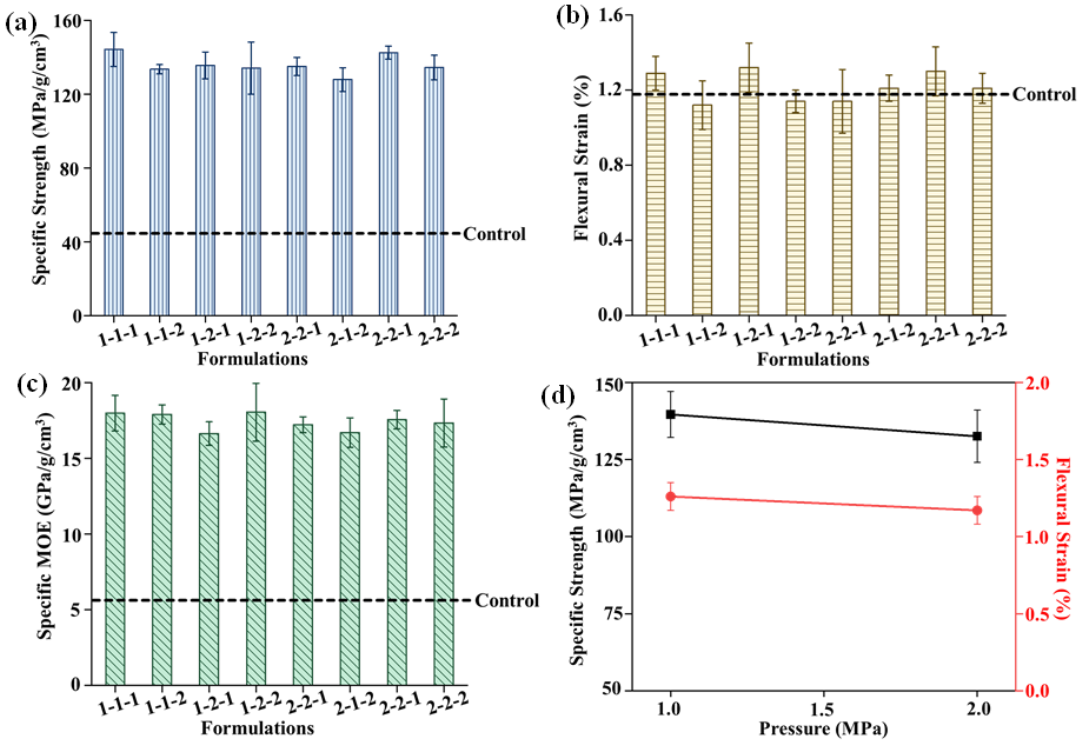

Figure 3.3: (a) Specific strength , (b) flexural strain, (c) specific MOE data of the developed CNF laminated containers measured in the parallel to grain direction, (d) relationship of specific strength and flexural strain with pressure in the parallel direction of the wood fiber alignment.

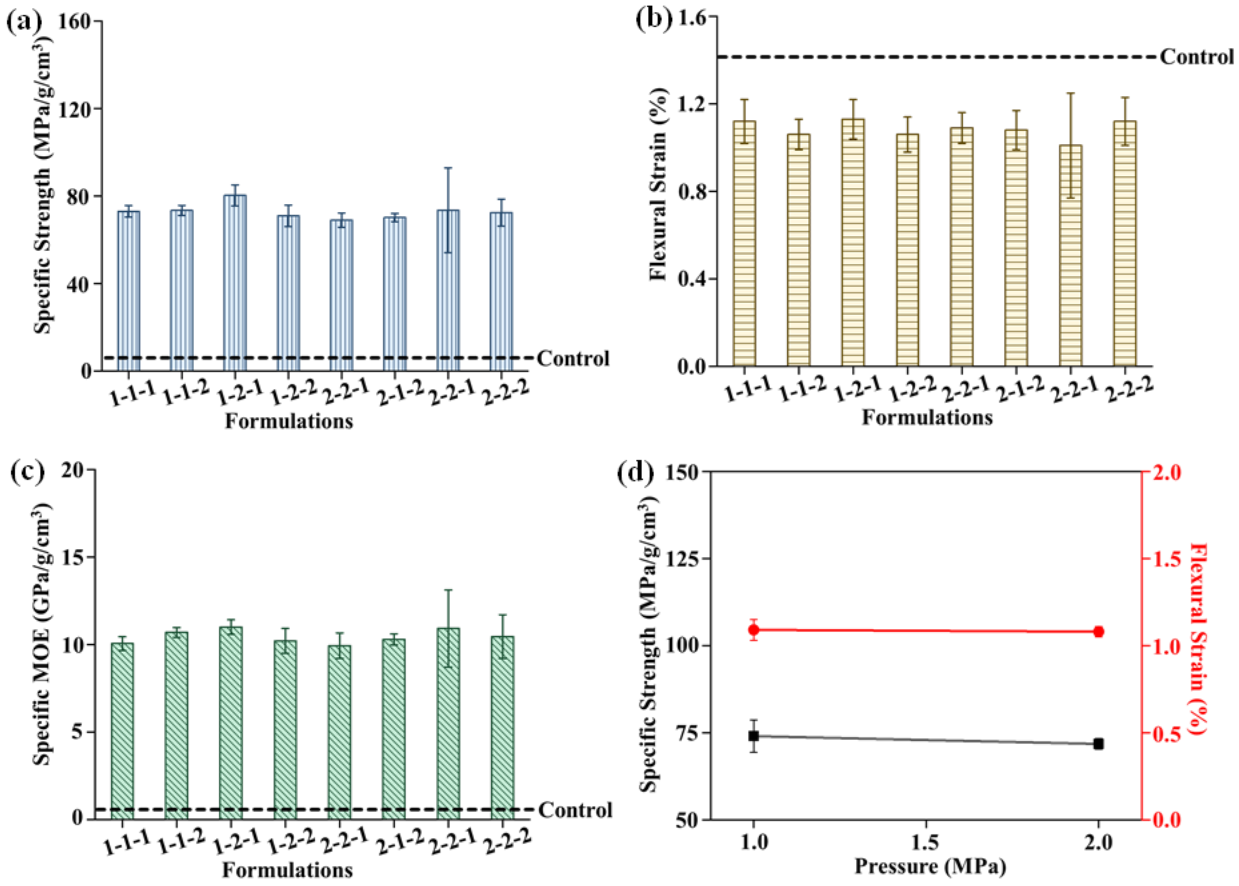

Figure 3.4: (a) Specific strength, (b) flexural strain, and (c) specific MOE data of the developed CNF laminated containers in the perpendicular to grain direction, (d) relationship of specific strength and flexural strain with pressure in the perpendicular direction of the wood fiber alignment.

The composite material was also found to be flexible in nature. In the parallel direction of the composite, the highest strain value was achieved for the formulation 1-2-1 (1.32 ± 0.13%) while the lowest value was found for the formulation 1-1-2 (1.12 ± 0.13%)(Figure 3.3 (b)). A statistically significant difference was found between the highest and the lowest strain values. The factorial design of the formulation demonstrated that pressure and interaction of time and temperature have a significant effect on the flexural strain values of the formulations in the parallel to grain direction. In the perpendicular direction, there was no statistical significance of

difference found between the highest and lowest values of the flexural strain (Figure 3.4 (b)).The specific MOE values in both parallel and perpendicular direction did not show any statistical difference among them (Figure 3.3 (c) and Figure 3.4 (c), respectively).

The specific flexural strength, flexural strain and specific MOE values significantly increased after adding the CNF layers on the wood veneer. Wood is inherently stronger in the growth direction (fiber alignment direction)(Ross, 2021). The addition of dense CNF layers having higher mechanical properties to wood veneer provides the specimens with higher mechanical properties in the parallel to grain direction. From Figure 3.3(d), a decreasing trend of mechanical properties is also found with increasing pressure. One possible reason could be the presence of small cracks (deep lathe checks) in between the fibers of the wood veneers cut using by rotary peeling where the depth of the lathe check could be up to 90% of the veneer thickness. Previous studies showed that these checks could open below 1 MPa pressure and affect the mechanical properties of the veneer (Rohumaa et al., 2013). However, the percentages of lathe check in the wood veneer was not measured in this study as the veneers were laminated by CNF films.

As expected, the specific flexural strength and specific MOE values of the samples were much higher than those of the control sample. However, the control sample achieved higher flexural strain values than the composite specimens. As the strength and stiffness of the sample increased significantly, it is expected that the flexibility of the sample would be compromised. In the perpendicular direction, no significant difference was found in the overall flexural properties among the formulation due to pressure changes

3.3.2. Lamination Quality

The lamination on food serving containers developed in this work plays a crucial role not only in mechanical and barrier properties but also for aesthetics. The adhesion properties between the

laminated layers ensure hygiene, food safety and prevent detrimental food contamination. The adhesion properties of the CNF laminated food container were characterized through the measurement of peel strength between the adherend layers.

Figure 3.5 indicates the outcomes of maximum peel strength value of the formulations. The highest peel strength value (25.6 N/mm) was achieved by formulation 1-1-1. The formulation 2-2-2 demonstrated the lowest peel strength (7.9 N/mm). The peel strength between the adhered layers also varied with the treatment factors (temperature, pressure, and press time). The interaction of time and pressure had a significant effect on the peel strength values.

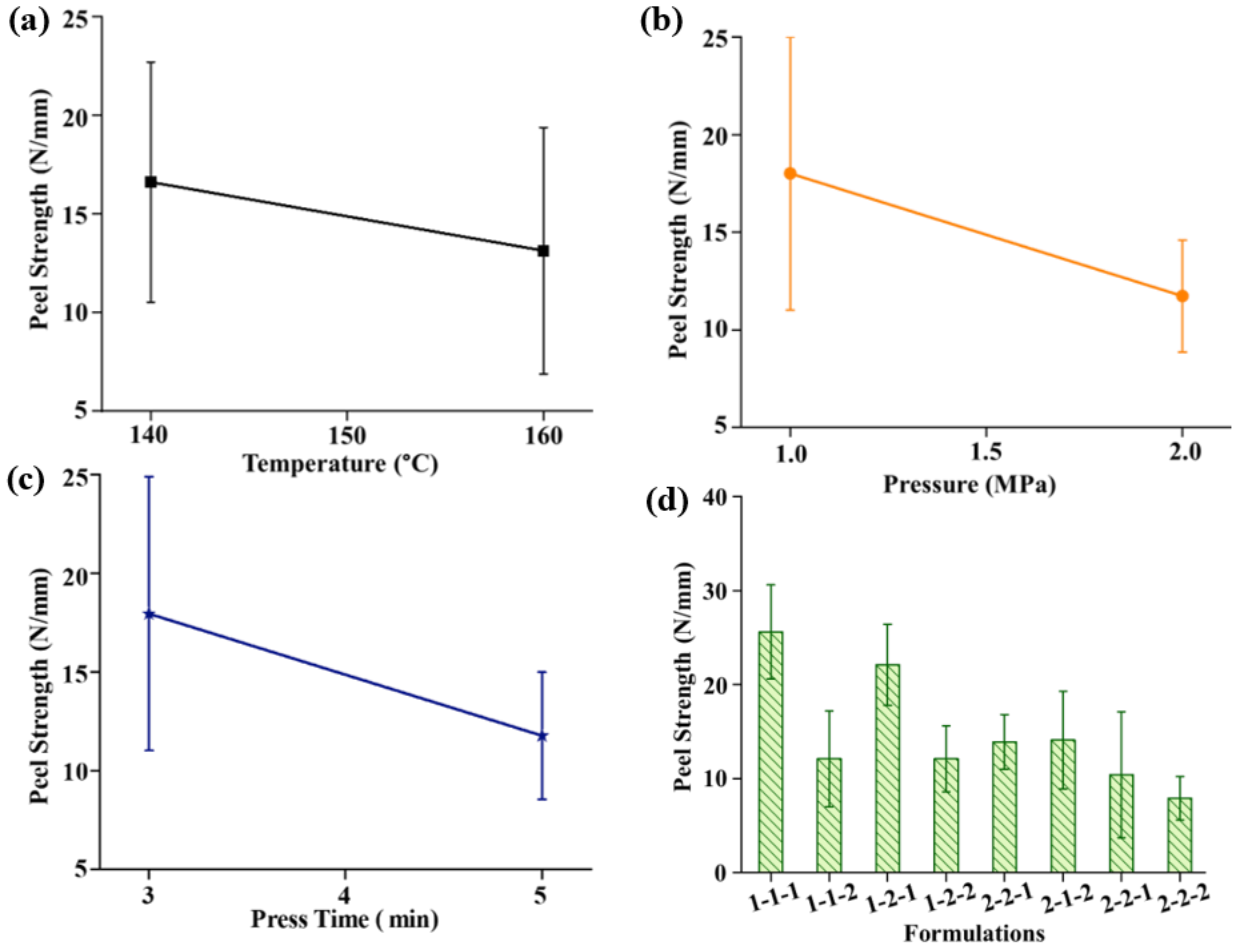

Figure 3.5: The relationship of peel strength with (a) temperature, (b) pressure, (c) time, and (d) specific peel strength of the formulations.

An increase in treatment factors led to a decrease in peel strength. The samples pressed for 3 minutes at 140°C and 1 MPa exhibited the highest peel resistance. Conversely, samples pressed for 5 minutes at a higher temperature of 160°C and 2 MPa showed less resistance to peel load. The reasons for decreasing peel resistance with increasing treatment factor levels are further investigated and discussed in the later sections.

3.3.3. Thermal properties

The thermal stability of food serving containers plays a vital role in ensuring food safety, integrity, and convenience. That is why it is important to investigate the thermal stability of the component of food serving containers to prevent harmful chemical leaching in the food when exposed to higher temperatures. The thermal degradation temperature of the pure PAE (Polycup), pure CNF, and CNF with PAE were determined using thermogravimetric analysis (TGA) in air. Figure 3.6 (a) and (b) demonstrate the weight loss and the derivative weight loss (DTG) of the components with the increase in temperature. The main steps of thermal degradation are associated with the residual moisture evaporation and subsequently the chemical bond decomposition.

The onset temperature and peak temperature of pure PAE were observed at around 203°C and 274°C respectively. The decomposition of pure PAE resulted in the appearance of initial and major degradation peaks at close temperature changes indicate degradation by pyrolysis and oxidation of the PAE as tested was done in air.

In TGA, the onset temperature for thermal degradation of CNFs was found to be about 223°C with a peak temperature of 338°C. The CNF film used for the TGA analysis was prepared by hot pressing at 160°C. During the thermal degradation of CNFs, processes like oxidation, depolymerization, and dehydration took place, along with the production of volatile compounds.

The higher thermal degradation temperature of CNF film can be achieved by heat treatment due to stable hydrogen bond formation (Tao et al., 2019; Xia et al., 2018; Yang et al., 2007). Additionally, CNF can attain crystallinity when heat-dried, as the heat drying process can transform some portions of the amorphous and para-crystalline regions of CNF into regular crystalline structures. This increase in crystallinity contributes to the thermal stability of CNFs (Chen et al., 2011; Tao et al., 2019).

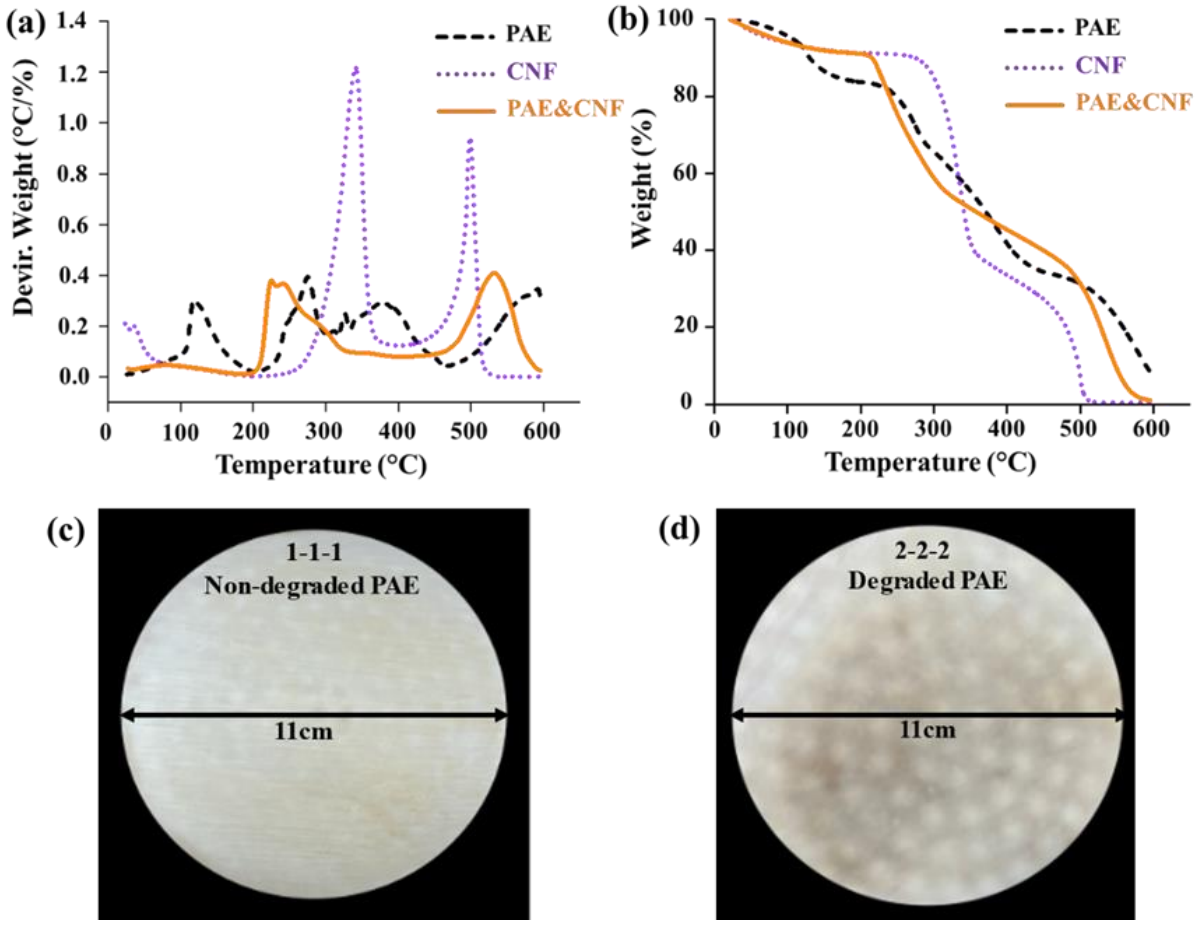

Figure 3.6: Representative (a) DTG curves, and (b) TGA curves of the components of the lamination as a function of temperature. (c) 1-1-1 sample with no Polycup degradation, (b) 2-2-2 sample with a sign of Polycup degradation.

The crosslinked CNF with PAE showed less thermal stability than un-crosslinked CNF films. The onset temperature for crosslinked CNF film in TGA was around 186°C and peak

temperature was 234°C. In Figure 3.6 (c-d), the images for formulations 1-1-1 (at 140°C ,1 MPa for 3 min pressed) and 2-2-2 (at 160°C, 2 MPa for 5 min pressed) are represented. The low peel strength observed at higher pressure levels may be attributed to the increased interaction between CNF and Polycup during hot press, inducing degradation of Polycup even at lower temperatures. The samples also exhibited a dark brown color, indicating Polycup degradation. Previous studies showed that the formation of the ester bonds between CNF and Polycup (PAE) is responsible for thermal degradation of crosslinked CNF at lower temperatures (Dehabadi & Wilson, 2014; González-Ugarte et al., 2020).

3.3.4. Surface Morphology

SEM imaging was conducted at various magnifications to study the surface morphology of the composite's bonded layers. Furthermore, images of unlaminated wood veneer were captured to facilitate a comparison between the laminated and unlaminated wood veneer surfaces. The images presented in Figure 3.7 (a-c) represents the microscale surface of unlaminated wood veneer, where noticeable pores at the surface act as channels for the movement of oil and water through the wood veneer.

In Figure 3.7 (d-f) and (j-l), SEM images of adhesive-bonded CNF film are displayed for formulations 1-1-1 and 2-2-2 respectively. Both CNF film surfaces appear almost identical after undergoing peel tests. Upon examining the microscale SEM image, it is noticeable that the CNFs are randomly aligned on the wood veneer surface, consistent with the natural behavior of CNFs. Importantly, no wood fibers were observed to be adhered to the CNF surface, indicating an absence of wood failure during the peel test.

Images of wood veneer strips after peeling from the CNF layer are shown in Figure 3.7 (g-i and m-o). The microscale images suggest that more CNF fibers remain on the veneer's surface for

formulation 2-2-2 than for formulation 1-1-1. This observation is consistent with the lower peel strength test results obtained from the composites for the formulation 2-2-2. Most of the surface of the wood veneer for all formulations remained clean, indicating that most of the CNF fibers remained at the surfaces of the CNF films. The SEM images identified no substantial evidence of cohesive failure of the composites. It is possible that the reduced peel resistance observed in formulation 2-2-2 is due to the adhesive penetrating too highly into the wood veneer at high pressure (2 MPa), resulting in a starved glue line that weakens the bonding strength between the layers. The lower peel strength can also result from higher surface roughness of the wood

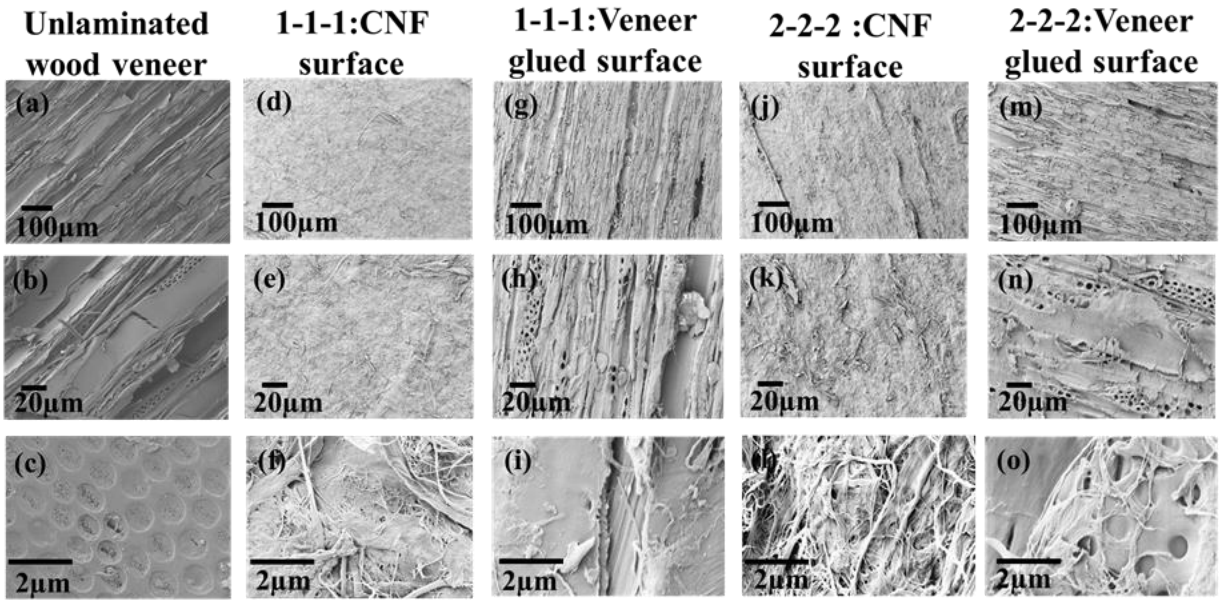

Figure 3.7: SEM images of (a-c) unlaminated wood veneer, and (d-f) glued CNF surface of the formulation 1-1-1, (g-i) glued wood veneer surface of the formulation 1-1-1, (j-l) glued CNF surface of the formulation 2-2-2, (m-o) glued wood veneer surface of the formulation 2-2-2 after peel test.

3.3.5. Oil and grease resistance

Food serving containers require excellent oil and grease barrier properties for optimal food protection, preservation, and presentation, all while maintaining nutritional value and edibility. All formulations in this study passed kit number 12, the most aggressive reagent. This result

aligns with the kit test results of CNF-coated molded pulp containers and wood flour composites (Hossain et al., 2021; J. Zhang & Youngblood, 2023). The high density and internal hydrogen bonds of CNF-coated surfaces explain their excellent oil and grease barrier properties when cellulosic surfaces are dried in contact (Hubbe & Pruszynski, 2020). The hydrogen bonding and van der Waals interactions between the molecules of CNFs contribute to forming denser structures with lower porosity, thus reducing air penetration. The decreased air penetration is directly related to the grease resistance of the coated CNF surface (Aulin et al., 2010; Tyagi et al., 2021).

The hydrophilic nature of CNF also prevents the formation of strong bonds with oil molecules, making CNF coating an effective oil and grease barrier (Hubbe et al., 2017). The CNF networks are intricate and prevent oil and grease from penetrating between the layers (Hossain et al., 2021). Commercial paper plates typically have porous structures on their surfaces due to their interwoven fiber arrangement, which can act as passages for oil and grease. In contrast, CNF coating provides a smoother surface finish with less porosity, resulting in a higher kit value compared to the commercial paper plate's kit value of 4 (Tayeb et al., 2020; Jung et al., 2018).

3.3.6. Water Resistance

Water absorptiveness (Cobb value) helps determine the amount of water absorbed by the food serving container for a certain time. Cobb values of layered composites (1-2-1 and 2-1-2), and commercial paper plate are presented in Figure 3.8.

For hot-pressed wood veneer, water absorption values were significantly higher than the commercial plates for 1200 s. A significant amount of variability was also observed in the Cobb values of pressed wood veneer. However, after adding two layers of CNF films on the top and bottom of the wood veneer, the Cobb values and variability were reduced significantly. The

composite made by hot-pressing at 140℃, 1 MPa, and 3 min (formulation 1-2-1) showed significantly higher water absorption values than commercial plates, whereas at 160℃, 2 MPa, and 5 min hot pressing (formulation 2-1-2), the Cobb value was not statistically different from the paper-based commercial containers.

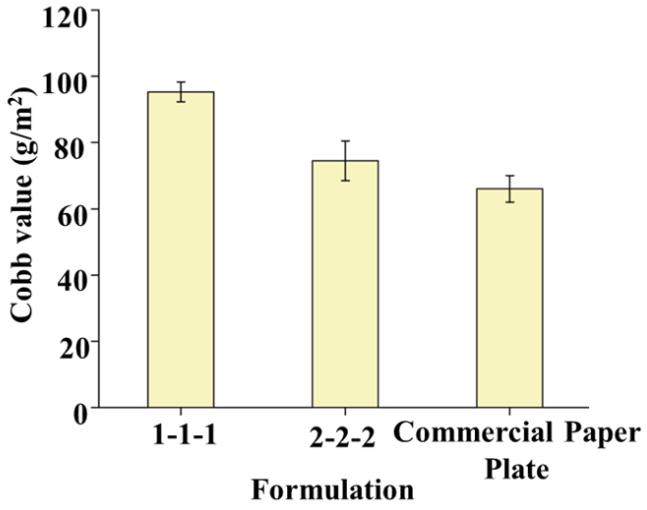

Figure 3.8: Cobb values of the prepared food serving containers and a comparison with commercially available plates.

As shown in Figure 3.9 (a), semicrystalline cellulose nanofibrils form an extensive internal network by connecting through hydrogen bonds between hydroxyl and hydroxymethyl groups, which leads to a compact film structure (Hinterstoisser & Salmén, 2000; Pinkert et al., 2009). When CNF films are made by filtration, they are more likely to have interfibrillar agglomeration. This is due to a high number of hydrogen bonds in vacuum-filtered films, rendering them highly susceptible to humidity (Benítez et al., 2013). Water enables the CNF films to plasticize, resulting in the fragmentation of hydrogen bonds between fibrils (Shimizu et al., 2016).

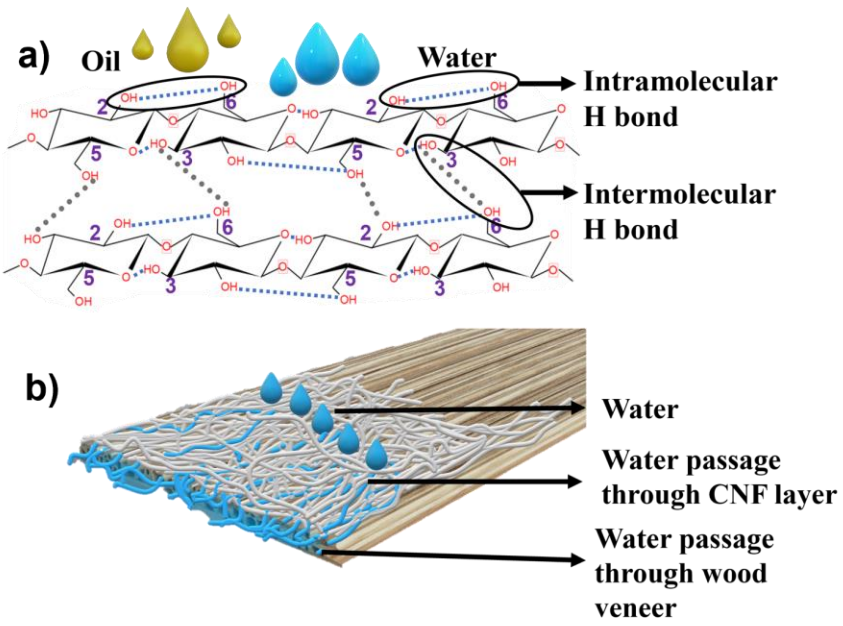

Figure 3.9: (a) Intramolecular and intermolecular hydrogen bonds of CNFs, (b) water absorption mechanism of the food serving container.

The water contact angle of CNF films, which is smaller than 90° due to the hydrophilic nature of the hydroxyl groups on the film's surface, facilitates water penetration through the film's surface. Thus, it makes a way to penetrate the water through the pores of the CNF film by capillary forces. Though water can be easily absorbed by the CNF layer, the flow path of water is very tortuous (shown in Figure 3.9 (b)) which causes an elongated water passage path and a longer retention time. For these reasons, the double-sided CNF laminated containers were found leak proof during the Cobb test when tested for 1200 s. It was also observed that the food containers generated under higher temperature, higher pressure and longer pressing time showed less water absorption values and showed less water passage than the container produced using lower temperature and pressure with shorter press time. Higher temperature and higher pressure reduce the porosity of the CNF film by densification when the film is dried by using a hot press and also promote cellulose hornification (Hasan et al., 2021). Water can have fewer channels to

pass through the film with decreasing porosity, which aligned with the Cobb test values of the composites in this study. Finally, in natural wood, trees have numerous transportation pores to pass nutrients and water. Long and plentiful micro channels are open in the thin rotary cut wood veneer with reduced thickness which are suitable for water passages (also observed in the SEM image) (Zhu et al., 2021). For this reason, it was not possible to measure the Cobb values of the unlaminated wood veneers as water seeped through them very quickly.

3.4. Conclusions

This study presented a novel food container design that utilized CNF layers on both sides of a yellow birch wood veneer and bonded together using food-grade Polycup. These samples were hot pressed at varying temperatures, pressures, and press times. The control samples were prepared by pressing wood veneer at 160℃ and 2 MPa for 5 minutes without lamination and were compared with the composite samples of identical formulation in terms of mechanical properties. All composite samples showed significant improvements in both flexural strength and MOE values. In particular, the composite sample exhibited 1.8 times greater flexural strength in the parallel direction and a remarkable 30 times higher strength in the perpendicular direction of wood fibers compared to the control samples for our best formulation. Furthermore, the addition of CNF layers to the wood veneer increased the MOE values of the composite sample by 1.8 times in the parallel direction and impressively 40 times when tested in the perpendicular direction to the wood fibers alignment. It is vital to note that the flexural strain of the container sample only slightly increased in the parallel direction (by 2%), however it reduced in the perpendicular direction (by 30%). This outcome was expected, considering the higher increase in flexural strength observed in the perpendicular to grain direction. The peel strength of the formulation with lower levels of treatment factors was 2.2 times more than the formulations with

higher levels of treatment factors. To shed more light on these findings, the study used SEM to investigate the surface morphology of the peeled samples and thermogravimetric analysis to evaluate the thermal degradation of CNF and Polycup. The images from the SEM did not reveal any significant CNF layer or wood veneer failure, indicating that the failure mode was largely adhesive failure. On the other hand, the TGA data showed that thermal degradation of CNF when bonded with Polycup initiated at a lower temperature which could be due to ester bond formation during CNF-Polycup crosslinking.

The CNF-wood veneer composites developed in this work outperformed commercial paper plates in their resistance to oil and grease, as demonstrated by Kit number 12 versus Kit number 4. When prepared at 160°C and 2 MPa for 5 minutes, this composite showed no noteworthy disparity in water absorption tendency as compared to commercial paper plates that contained PFAs.

Overall, this work highlights the potential for CNF lamination to improve the mechanical and barrier properties of food serving containers made of wood veneer. This CNF-laminated wood veneer food serving container may provide a long-term solution to the challenges associated with conventional wood veneer-based containers. This study also presents an efficient method for readily producible and easily compostable food serving containers, which can be used as a safe and effective alternative to per- and polyfluoroalkyl compounds (PFAs)-containing containers, and therefore contributing to sustainable-practices.

CHAPTER 4

CONCLUSIONS AND FUTURE RESEARCH DIRECTION

4.1. Conclusions

The overall thesis is focused on developing oriented CNF films and CNF film-laminated containers for high barrier food packaging products with enhanced mechanical properties. The conclusions of this thesis were drawn from the findings and discussions mentioned in the previous chapters, and are presented below:

I. It is possible to produce oriented CNF films using an auto dynamic sheet former (ADSF) and careful induced shrinkage drying. Optimizing the wire speed in the ADSF can improve the mechanical strength and stiffness of Z_Z drying-produced films, as compared to non-restrained XY_Z drying. The optimized wire speed resulted in films with higher anisotropy ratios, leading to improved oxygen barrier performance. The XY_Z films outperformed the Z_Z films in this aspect, although the differences between the values were not significant. In spite of polarized light microscopy (PLM) offers localized insight into orientation, the anisotropy ratio and differences in barrier properties remain significant indicators of film orientation. The study found that there is an interaction between wire speed and CNF solids content, which can result in the formation of large, well-aligned CNF sheets. It also highlights the importance of shrinkage drying and fiber orientation in improving the mechanical and barrier properties of CNF films.

II. This research introduced an innovative food container design that combines CNF layers with wood veneer, bonded using a food-grade PAE. The properties of this composite were compared to those of wood veneer-based and commercial paper-based containers.

The results showed significant improvements in flexural strength and MOE values in both parallel and perpendicular directions to the wood grain, when compared to wood veneer containers. The study also found that the peel resistance between the layers depends on the processing conditions. Thermogravimetric analysis (TGA) revealed that CNF-PAE crosslinking could degrade at a lower temperature. Additionally, compared to conventional paper plates, CNF-wood veneer composites displayed superior oil and grease resistance with no significant difference in water resistance. This research confirms that CNF lamination is an effective way to enhance the structural and barrier integrity of wood veneer-based food containers.

4.2. Future Work

I. This study only considered two processing parameters while produced films using the ADSF: CNF solids content and wire speed. Further investigation can be conducted to improve the alignment and mechanical strength of ADSF-produced films by modifying the nozzle geometry, nozzle diameter, and suspension flow rate.

II. During oxygen barrier testing, it was observed that the ADSF-produced CNF films formed non-uniformly and contained numerous pinholes, leading to test failures. Further research is needed to improve the dispersion of CNF fibers and ensure uniform sheet thickness during film formation.

III. Although mechanical and oxygen barrier testing provided indications of alignment in the films, polarized light microscopy may not be sufficient in analyzing the degree of alignment for a significant portion of the films. Therefore, additional research is necessary to explore more effective methods for testing alignment, such as imaging or indirect measures.

IV. Additional research is needed to examine the mechanical and barrier qualities of multi-layer food serving container, with a focus on the impact of CNF film and wood veneer basis weight. Furthermore, exploring strategies to improve water resistance and reduce moisture sensitivity would be beneficial in enhancing container performance.

V. The investigation of sustainability and storage under varying weathering conditions is a crucial aspect in comprehending the durability of food takeout containers. Furthermore, the examination of the process and time frame in which microorganism disintegration occurs within the composite material may shed light on its potential compostability.

VI. Additional research can be conducted to explore the potential for shaping the composite material into three-dimensional forms that are suitable for use as closed food takeout containers. It is also important to assess the market viability and cost-effectiveness of producing this CNF-wood veneer container to determine its potential as a replacement for PFAs and plastic-based food containers.

REFERENCES

Amini, E., Hafez, I., Tajvidi, M., & Bousfield, D. W. (2020). Cellulose and lignocellulose nanofibril suspensions and films: A comparison. *Carbohydrate Polymers*, *250*, 117011. https://doi.org/10.1016/j.carbpol.2020.117011

ASTM, D. (1876). Standard test method for peel resistance of adhesives (T-peel test). *Volume*, *15*, 105–107.

Aulin, C., Gällstedt, M., & Lindström, T. (2010). Oxygen and oil barrier properties of microfibrillated cellulose films and coatings. *Cellulose*, *17*, 559–574.

Benítez, A. J., Torres-Rendon, J., Poutanen, M., & Walther, A. (2013). Humidity and multiscale structure govern mechanical properties and deformation modes in films of native cellulose nanofibrils. *Biomacromolecules*, *14*(12), 4497–4506.

Bharadwaj, R. K. (2002). Effect of H2O on the diffusion of N2 in PMMA: A molecular dynamics simulation study. *Macromolecules*, *35*(13), 5334–5336.

Chen, Y., Wan, J., Huang, M., Ma, Y., Wang, Y., Lv, H., & Yang, J. (2011). Influence of drying temperature and duration on fiber properties of unbleached wheat straw pulp. *Carbohydrate Polymers*, *85*(4), 759–764.

Chowdhury, R. A., Nuruddin, M., Clarkson, C., Montes, F., Howarter, J., & Youngblood, J. P. (2018). Cellulose nanocrystal (CNC) coatings with controlled anisotropy as high-performance gas barrier films. *ACS Applied Materials & Interfaces*, *11*(1), 1376–1383.

D3985-05, A. (2010). Standard test method for oxygen gas transmission rate through plastic film and sheeting using a coulometric sensor. In *ASTM, Annual Book of ASTM*. ASTM international Philadelphia, PA, USA.

Debeaufort, F. (2021). Wood-based Packaging. *Packaging Materials and Processing for Food, Pharmaceuticals and Cosmetics*, 1.

Debnath, M., Sarder, R., Pal, L., & Hubbe, M. A. (2022). Molded Pulp Products for Sustainable Packaging: Production Rate Challenges and Product Opportunities. *BioResources*, *17*(2).

Dehabadi, L., & Wilson, L. D. (2014). Polysaccharide-based materials and their adsorption properties in aqueous solution. *Carbohydrate Polymers*, *113*, 471–479.

Didone, M., Saxena, P., Brilhuis-Meijer, E., Tosello, G., Bissacco, G., Mcaloone, T. C., Pigosso, D. C. A., & Howard, T. J. (2017). Moulded pulp manufacturing: Overview and prospects for the process technology. *Packaging Technology and Science*, *30*(6), 231–249.

Dlubek, G., Redmann, F., & Krause-Rehberg, R. (2002). Humidity-induced plasticization and antiplasticization of polyamide 6: A positron lifetime study of the local free volume. *Journal of Applied Polymer Science*, *84*(2), 244–255.

Ebnesajjad, S. (2012). *Plastic films in food packaging: Materials, technology and applications*. William Andrew.

Fujisawa, S., Togawa, E., & Hayashi, N. (2016). Orientation control of cellulose nanofibrils in all-cellulose composites and mechanical properties of the films. *Journal of Wood Science*, *62*, 174–180.

Fukuya, M. N., Senoo, K., Kotera, M., Yoshimoto, M., & Sakata, O. (2014). Enhanced oxygen barrier property of poly (ethylene oxide) films crystallite-oriented by adding cellulose single nanofibers. *Polymer*, *55*(22), 5843–5846.

Gallego-Schmid, A., Mendoza, J. M. F., & Azapagic, A. (2019). Environmental impacts of takeaway food containers. *Journal of Cleaner Production*, *211*, 417–427.

Geueke, B., Phelps, D. W., Parkinson, L. V., & Muncke, J. (2023). Hazardous chemicals in recycled and reusable plastic food packaging. *Cambridge Prisms: Plastics*, *1*, e7.

Geyer, R., Jambeck, J. R., & Law, K. L. (2017). Production, use, and fate of all plastics ever made. *Science Advances*, *3*(7), e1700782.

Ghasemi, S., Rahimzadeh-Bajgiran, P., Tajvidi, M., & Shaler, S. M. (2020). Birefringence-based orientation mapping of cellulose nanofibrils in thin films. *Cellulose*, *27*, 677–692.

Ghasemi, S., Tajvidi, M., Bousfield, D. W., Gardner, D. J., & Gramlich, W. M. (2017). Dry-Spun Neat Cellulose Nanofibril Filaments: Influence of Drying Temperature and Nanofibril Structure on Filament Properties. *Polymers*, *9*(9), Article 9. https://doi.org/10.3390/polym9090392

Gigac, J., & Fišerová, M. (2010). Effect of velocity gradient on papermaking properties. *Cellulose Chemistry & Technology*, *44*(9), 389.

Gindl, W., & Keckes, J. (2007). Drawing of self-reinforced cellulose films. *Journal of Applied Polymer Science*, *103*(4), 2703–2708.

Gindl-Altmutter, W., Veigel, S., Obersriebnig, M., Tippelreither, C., & Keckes, J. (2012). High-modulus oriented cellulose nanopaper. In *Functional materials from renewable sources* (pp. 3–16). ACS Publications.

González-Ugarte, A. S., Hafez, I., & Tajvidi, M. (2020). Characterization and properties of hybrid foams from nanocellulose and kaolin-microfibrillated cellulose composite. *Scientific Reports*, *10*(1), 17459.

Greaseproof Paper Market Size, Share, Trends | Forecast 2025. (n.d.). Retrieved October 26, 2023, from https://www.acumenresearchandconsulting.com/greaseproof-paper-market

H. Tayeb, A., Tajvidi, M., & Bousfield, D. (2020). Paper-Based Oil Barrier Packaging using Lignin-Containing Cellulose Nanofibrils. *Molecules*, *25*(6), Article 6. https://doi.org/10.3390/molecules25061344

Hasan, I., Wang, J., & Tajvidi, M. (2021). Tuning physical, mechanical and barrier properties of cellulose nanofibril films through film drying techniques coupled with thermal compression. *Cellulose*, *28*, 11345–11366.

Hinterstoisser, B., & Salmén, L. (2000). Application of dynamic 2D FTIR to cellulose. *Vibrational Spectroscopy*, *22*(1–2), 111–118.

Horton, A. A., Walton, A., Spurgeon, D. J., Lahive, E., & Svendsen, C. (2017). Microplastics in freshwater and terrestrial environments: Evaluating the current understanding to identify the knowledge gaps and future research priorities. *Science of the Total Environment*, *586*, 127–141.

Hossain, R., Tajvidi, M., Bousfield, D., & Gardner, D. J. (2021). Multi-layer oil-resistant food serving containers made using cellulose nanofiber coated wood flour composites. *Carbohydrate Polymers*, *267*, 118221. https://doi.org/10.1016/j.carbpol.2021.118221

Hubbe, M. A., Ferrer, A., Tyagi, P., Yin, Y., Salas, C., Pal, L., & Rojas, O. J. (2017). Nanocellulose in thin films, coatings, and plies for packaging applications: A review. *BioResources*, *12*(1), 2143–2233.

Hubbe, M. A., & Pruszynski, P. (2020). Greaseproof paper products: A review emphasizing ecofriendly approaches. *BioResources*, *15*(1), 1978–2004.

Isogai, A. (2018). Development of completely dispersed cellulose nanofibers. *Proceedings of the Japan Academy, Series B*, *94*(4), 161–179.

Johnson, D., Papadis, M., Bilodeau, M., Crossley, B., Foulger, M., & Gelinas, P. (2016). Effects of cellulosic nanofibrils on papermaking properties of fine papers. *TAPPI Journal*, *15*, 395–402. https://doi.org/10.32964/TJ15.6.395

Jonoobi, M., Oladi, R., Davoudpour, Y., Oksman, K., Dufresne, A., Hamzeh, Y., & Davoodi, R. (2015). Different preparation methods and properties of nanostructured cellulose from various natural resources and residues: A review. *Cellulose*, *22*, 935–969.

Jost, V., Kobsik, K., Schmid, M., & Noller, K. (2014). Influence of plasticiser on the barrier, mechanical and grease resistance properties of alginate cast films. *Carbohydrate Polymers*, *110*, 309–319.

Jung, J., Kasi, G., & Seo, J. (2018). Development of functional antimicrobial papers using chitosan/starch-silver nanoparticles. *International Journal of Biological Macromolecules*, *112*, 530–536.

Kjellgren, H., Gällstedt, M., Engström, G., & Järnström, L. (2006). Barrier and surface properties of chitosan-coated greaseproof paper. *Carbohydrate Polymers*, *65*(4), 453–460.

Klemm, D., Heublein, B., Fink, H.-P., & Bohn, A. (2005). Cellulose: Fascinating Biopolymer and Sustainable Raw Material. *Angewandte Chemie International Edition*, *44*(22), 3358–3393. https://doi.org/10.1002/anie.200460587

Kouko, J., & Retulainen, E. (2018). The relationship between shrinkage and elongation of bleached softwood kraft pulp sheets. *Nordic Pulp & Paper Research Journal*, *33*(3), 522–533.

Li, K., Clarkson, C. M., Wang, L., Liu, Y., Lamm, M., Pang, Z., Zhou, Y., Qian, J., Tajvidi, M., & Gardner, D. J. (2021). Alignment of cellulose nanofibers: Harnessing nanoscale properties to macroscale benefits. *ACS Nano*, *15*(3), 3646–3673.

Mariano, M., El Kissi, N., & Dufresne, A. (2014). Cellulose nanocrystals and related nanocomposites: Review of some properties and challenges. *Journal of Polymer Science Part B: Polymer Physics*, *52*(12), 791–806. https://doi.org/10.1002/polb.23490

Markatos, D. N., Sarakinis, A., & Mavrilas, D. (2018). Tuning fiber alignment to achieve mechanical anisotropy on polymeric electrospun scaffolds for cardiovascular tissue engineering. *J. Mater. Sci. Eng*, *7*(4), 466.

Moon, R. J., Martini, A., Nairn, J., Simonsen, J., & Youngblood, J. (2011). Cellulose nanomaterials review: Structure, properties and nanocomposites. *Chemical Society Reviews*, *40*(7), 3941–3994. https://doi.org/10.1039/C0CS00108B

Mörseburg, K., & Chinga-Carrasco, G. (2009). Assessing the combined benefits of clay and nanofibrillated cellulose in layered TMP-based sheets. *Cellulose*, *16*, 795–806.

Mousavi, S. M. M., Afra, E., Tajvidi, M., Bousfield, D. W., & Dehghani-Firouzabadi, M. (2018). Application of cellulose nanofibril (CNF) as coating on paperboard at moderate solids content and high coating speed using blade coater. *Progress in Organic Coatings*, *122*, 207–218.

Muramatsu, M., Okura, M., Kuboyama, K., Ougizawa, T., Yamamoto, T., Nishihara, Y., Saito, Y., Ito, K., Hirata, K., & Kobayashi, Y. (2003). Oxygen permeability and free volume hole size in ethylene–vinyl alcohol copolymer film: Temperature and humidity dependence. *Radiation Physics and Chemistry*, *68*(3–4), 561–564.

Nair, S. S., Zhu, J. Y., Deng, Y., & Ragauskas, A. J. (2014). High performance green barriers based on nanocellulose. *Sustainable Chemical Processes*, *2*, 1–7.

Nazari, B., Kumar, V., Bousfield, D. W., & Toivakka, M. (2016). Rheology of cellulose nanofibers suspensions: Boundary driven flow. *Journal of Rheology*, *60*(6), 1151–1159.

Ncube, L. K., Ude, A. U., Ogunmuyiwa, E. N., Zulkifli, R., & Beas, I. N. (2020). Environmental Impact of Food Packaging Materials: A Review of Contemporary Development from Conventional Plastics to Polylactic Acid Based Materials. *Materials*, *13*(21), Article 21. https://doi.org/10.3390/ma13214994

Olsson, E., Johansson, C., Larsson, J., & Järnström, L. (2014). Montmorillonite for starch-based barrier dispersion coating—Part 2: Pilot trials and PE-lamination. *Applied Clay Science*, *97*, 167–173.

Osterberg, M., Vartiainen, J., Lucenius, J., Hippi, U., Seppälä, J., Serimaa, R., & Laine, J. (2013). A fast method to produce strong NFC films as a platform for barrier and functional materials. *ACS Applied Materials & Interfaces*, *5*(11), 4640–4647.

Peng, J., Ellingham, T., Sabo, R., Clemons, C. M., & Turng, L.-S. (2015). Oriented polyvinyl alcohol films using short cellulose nanofibrils as a reinforcement. *Journal of Applied Polymer Science*, *132*(48).

Petroudy, S. R. D., Garmaroody, E. R., & Rudi, H. (2017). Oriented cellulose nanopaper (OCNP) based on bagasse cellulose nanofibrils. *Carbohydrate Polymers*, *157*, 1883–1891.

Pinkert, A., Marsh, K. N., Pang, S., & Staiger, M. P. (2009). Ionic liquids and their interaction with cellulose. *Chemical Reviews*, *109*(12), 6712–6728.

Plastic Container Market Worth $112.5 Billion By 2025 | CAGR: 4.0%. (n.d.). Retrieved October 26, 2023, from https://www.grandviewresearch.com/press-release/global-plastic-container-market

Razza, F., Fieschi, M., Degli Innocenti, F., & Bastioli, C. (2009). Compostable cutlery and waste management: An LCA approach. *Waste Management*, *29*(4), 1424–1433.

Ritchie, R. O. (2011). The conflicts between strength and toughness. *Nature Materials*, *10*(11), 817–822.

Rohumaa, A., Hunt, C. G., Hughes, M., Frihart, C. R., & Logren, J. (2013). The influence of lathe check depth and orientation on the bond quality of phenol-formaldehyde–bonded birch plywood. *Holzforschung*, *67*(7), 779–786.

Ross, R. J. (2021). *Wood handbook: Wood as an engineering material*.

Rustagi, N., Pradhan, S. K., & Singh, R. (2011). Public health impact of plastics: An overview. *Indian Journal of Occupational and Environmental Medicine*, *15*(3), 100–103. https://doi.org/10.4103/0019-5278.93198

Sehaqui, H., Ezekiel Mushi, N., Morimune, S., Salajkova, M., Nishino, T., & Berglund, L. A. (2012). Cellulose nanofiber orientation in nanopaper and nanocomposites by cold drawing. *ACS Applied Materials & Interfaces*, *4*(2), 1043–1049.

Shimizu, M., Saito, T., & Isogai, A. (2016). Water-resistant and high oxygen-barrier nanocellulose films with interfibrillar cross-linkages formed through multivalent metal ions. *Journal of Membrane Science*, *500*, 1–7.

Su, Y., Yang, B., Liu, J., Sun, B., Cao, C., Zou, X., Lutes, R., & He, Z. (2018). Prospects for replacement of some plastics in packaging with lignocellulose materials: A brief review. *BioResources*, *13*(2), 4550–4576.

Sunny, T., Pickering, K. L., & McDonald-Wharry, J. (2021). Improving the alignment of dynamic sheet-formed mats by changing nozzle geometry and their reinforcement of polypropylene matrix composites. *Journal of Composites Science*, *5*(9), 226.

Syverud, K., & Stenius, P. (2009). Strength and permeability of MFC films. *Cellulose*, *16*(1), 75–85.

Tajvidi, M., Gardner, D. J., & Bousfield, D. W. (2016). Cellulose nanomaterials as binders: Laminate and particulate systems. *Journal of Renewable Materials*, *4*(5), 365.

Tao, P., Wu, Z., Xing, C., Zhang, Q., Wei, Z., & Nie, S. (2019). Effect of enzymatic treatment on the thermal stability of cellulose nanofibrils. *Cellulose*, *26*, 7717–7725.

TAPPI. (2009). Water absorptiveness of sized (non-bibulous) paper, paperboard, and corrugated fiberboard (Cobb test). *T 441 Om-09*.

TAPPI, T. (2012). *559 cm-12. Grease resistance test for paper and paperboard*. TAPPI Press: Atlanta, GA, USA.

Tayeb, A. H., Amini, E., Ghasemi, S., & Tajvidi, M. (2018). Cellulose nanomaterials—Binding properties and applications: A review. *Molecules*, *23*(10), 2684.

Tucki, K., Orynycz, O., Wasiak, A., Gola, A., & Mieszkalski, L. (2022). Potential routes to the sustainability of the food packaging industry. *Sustainability*, *14*(7), 3924.

Tyagi, P., Gutierrez, J. N., Nathani, V., Lucia, L. A., Rojas, O. J., Hubbe, M. A., & Pal, L. (2021). Hydrothermal and mechanically generated hemp hurd nanofibers for sustainable barrier coatings/films. *Industrial Crops and Products*, *168*, 113582.

Tyagi, P., Lucia, L. A., Hubbe, M. A., & Pal, L. (2019). Nanocellulose-based multilayer barrier coatings for gas, oil, and grease resistance. *Carbohydrate Polymers*, *206*, 281–288. https://doi.org/10.1016/j.carbpol.2018.10.114

Von Moos, N., Burkhardt-Holm, P., & Köhler, A. (2012). Uptake and effects of microplastics on cells and tissue of the blue mussel Mytilus edulis L. after an experimental exposure. *Environmental Science & Technology*, *46*(20), 11327–11335.

Walker, T. R., & Fequet, L. (2023). Current trends of unsustainable plastic production and micro (nano) plastic pollution. *TrAC Trends in Analytical Chemistry*, 116984.

Wang, J., Gardner, D. J., Stark, N. M., Bousfield, D. W., Tajvidi, M., & Cai, Z. (2018). Moisture and oxygen barrier properties of cellulose nanomaterial-based films. *ACS Sustainable Chemistry & Engineering*, *6*(1), 49–70.

Wang, L., Chen, C., Wang, J., Gardner, D. J., & Tajvidi, M. (2020). 17 Cellulose nanofibrils versus cellulose nanocrystals: Comparison of performance in flexible multilayer films for packaging applications. *Food Packaging and Shelf Life*, *23*, 100464. https://doi.org/10.1016/j.fpsl.2020.100464

Whba, F., Mohamed, F., Idris, M. I., & Yahya, M. S. (2022). *Characterization of Cellulose Nanocrystalline (CNCs) Derived from Microcrystalline Cellulose (MCC) Synthesized Using Acid Hydrolysis Method*. https://www.researchsquare.com/article/rs-2078344/latest

Xia, J., Zhang, Z., Liu, W., Li, V. C. F., Cao, Y., Zhang, W., & Deng, Y. (2018). Highly transparent 100% cellulose nanofibril films with extremely high oxygen barriers in high relative humidity. *Cellulose*, *25*(7), 4057–4066. https://doi.org/10.1007/s10570-018-1843-y

Xu, X., Liu, F., Jiang, L., Zhu, J. Y., Haagenson, D., & Wiesenborn, D. P. (2013). Cellulose Nanocrystals vs. Cellulose Nanofibrils: A Comparative Study on Their Microstructures and Effects as Polymer Reinforcing Agents. *ACS Applied Materials & Interfaces*, *5*(8), 2999–3009. https://doi.org/10.1021/am302624t

Yang, H., Yan, R., Chen, H., Lee, D. H., & Zheng, C. (2007). Characteristics of hemicellulose, cellulose and lignin pyrolysis. *Fuel*, *86*(12–13), 1781–1788.

Yook, S., Park, H., Park, H., Lee, S.-Y., Kwon, J., & Youn, H. J. (2020). Barrier coatings with various types of cellulose nanofibrils and their barrier properties. *Cellulose*, *27*(8), 4509–4523. https://doi.org/10.1007/s10570-020-03061-5

Zabihzadeh Khajavi, M., Ebrahimi, A., Yousefi, M., Ahmadi, S., Farhoodi, M., Mirza Alizadeh, A., & Taslikh, M. (2020). 15 Strategies for Producing Improved Oxygen Barrier Materials Appropriate for the Food Packaging Sector. *Food Engineering Reviews*, *12*(3), 346–363. https://doi.org/10.1007/s12393-020-09235-y

Zhang, F. D., Pei, J. C., Li, J., Liu, W., & Zhou, C. X. (2014). The Effect of Speeds of Jet and Wire on the Physical Properties of Paper Sheets Forming in a Dynamic Sheet Former. *China Pulp and Paper*, *33*(6), 25–30.

Zhang, J., & Youngblood, J. P. (2023). Cellulose Nanofibril (CNF)-Coated PFAS-Free, Grease-Resistant All-Bio-Based Molded Pulp Containers for Food Packaging. *ACS Applied Polymer Materials*, *5*(7), 5696–5706.

Zhu, X., Hu, J., Liu, G., Xu, D., Wei, Y., Li, D., Chang, S., Li, X., & Liu, Y. (2021). Unique 3D interpenetrating capillary network of wood veneer for highly efficient cross flow filtration. *Journal of Materials Science*, *56*, 3155–3167.

BIOGRAPHY OF THE AUTHOR

Nabanita Das was raised in a loving joint family in the vibrant and historic port city of Chattogram, Bangladesh. In 2010, she graduated from Silver Bells Girls' High School, and in 2012, she attended Chittagong College to complete her secondary education. She pursued a bachelor's degree in chemical engineering and polymer science at Shajalal University of Science and Technology, graduating in 2019, motivated by her firm passion for learning. Nabanita's learning journey took an inspiring turn during her internship in the cement industry, where she became involved in the Geocycle Bangladesh project. Her interest was sparked by this effort, which aims to turn waste from diverse businesses into eco-friendly fuel. Its significant objectives of partially replacing fossil fuel consumption and lowering greenhouse gas emissions inspired her to devote herself to learning about affordable, long-lasting, and environmentally friendly materials. She became particularly interested in developing solutions to mitigate non-compostable waste products, harnessing the power of renewable nanomaterials. Motivated by her curiosity about the broader applications of these innovative materials, Nabanita decided to further her academic pursuit. In January 2022, she enrolled in the master's program in Bioproducts Engineering at the University of Maine's School of Forest Resources. She has served as a session co-chair at the TAPPI Nano Conference and the PDC CNM Forum this year. Nabanita is currently pursuing a Master of Science in Bioproducts Engineering at the University of Maine and is due to graduate in December 2023. After completing her degree, she plans to continue her research at LRN (Laboratory of Renewable Nanomaterials) by pursuing a Ph.D. in Bioproducts Engineering at the University of Maine.